

# Fossil HII Regions: Self-Limiting Star Formation at High Redshift

S. Peng Oh<sup>1</sup> & Zoltán Haiman<sup>2</sup>

<sup>1</sup>*Theoretical Astrophysics, Mail Code 130-33, Caltech, Pasadena, CA 91125, USA.*

<sup>2</sup>*Department of Astronomy, Columbia University, 550 West 120th Street, New York, NY 10027, USA.*

29 October 2018

## ABSTRACT

Recent results by the *WMAP* satellite suggest that the intergalactic medium was significantly reionized at redshifts as high as  $z \sim 17$ . At this early epoch, the first ionizing sources likely appeared in the shallow potential wells of mini-halos with virial temperatures  $T_{\text{vir}} < 10^4\text{K}$ . Once such an ionizing source turns off, its surrounding HII region Compton cools and recombines. Nonetheless, we show that the “fossil” HII regions left behind remain at high adiabats, prohibiting gas accretion and cooling in subsequent generations of mini-halos. Thus, early star formation is self-limiting. We quantify this effect to show that star formation in mini-halos cannot account for the bulk of the electron scattering opacity measured by *WMAP*, which must be due to more massive objects. We argue that gas entropy, rather than IGM metallicity, regulates the evolution of the global ionizing emissivity, and impedes full reionization until lower redshifts. We discuss several important consequences of this early entropy floor for reionization. It reduces gas clumping, curtailing the required photon budget for reionization. An entropy floor also prevents  $\text{H}_2$  formation and cooling, due to reduced gas densities: it greatly enhances feedback from UV photodissociation of  $\text{H}_2$ . An early X-ray background would also furnish an entropy floor to the entire IGM; thus, X-rays impede rather than enhance  $\text{H}_2$  formation. Future 21cm observations may probe the topology of fossil HII regions.

## 1 INTRODUCTION

The high optical depth  $\tau = 0.17 \pm 0.04$  detected by the Wilkinson Microwave Anisotropy Probe (*WMAP*) satellite has lent greater credence to the notion of an early period of star formation and reionization,  $z_r = 17 \pm 8$  (Kogut et al 2003; Spergel et al 2003). If indeed the first stars formed at high redshift  $z \sim 20$ , they are expected to form in mini-halos<sup>1</sup> with shallow potential wells, in which  $\text{H}_2$  cooling is dominant (Abel, Bryan & Norman 2000; Bromm, Coppi & Larson 2002). More massive halos with  $T_{\text{vir}} > 10^4\text{K}$ , in which collisional ionization and line cooling can operate, are expected to be very rare at these redshifts. Modulo the effects of UV feedback on  $\text{H}_2$  formation and cooling, stars forming in such halos could therefore play a dominant role in an early reionization epoch. A great deal of effort has gone into assessing the impact of UV feedback on  $\text{H}_2$  cooling, as well as the counter-vailing effects of positive feedback effects such as an early X-ray background (e.g., Haiman, Abel & Rees (2000); Ciardi, Ferrara & Abel (2000); Ricotti, Gnedin & Shull (2002); Machacek, Bryan & Abel (2001)).

The main point of this paper is that the population of mini-halos is likely to be considerably sparser than previously assumed. This is because mini-halo formation is strongly suppressed even inside the fossil HII regions of dead ionizing sources. Although such HII regions recombine and cool by Compton scattering with cosmic microwave background (CMB) photons, they cannot cool to back to the temperature of the undisturbed intergalactic medium (IGM). Strong Jeans mass filtering takes place (Gnedin 2000), and subsequent mini-halos will no longer be able to accrete gas due to the smoothing effects of finite gas pressure. *Thus, once any patch of the universe is ionized, it can no longer host any more mini-halos, even if it subsequently cools and recombines.* In effect, the birth of the first stars leads to the demise of the mini-halo population: only one generation of stars can form within these shallow potential wells.

While many authors have noted and commented on the Jeans mass filtering after full reionization (Bullock, Kravtsov & Weinberg 2000; Benson et al 2002; Somerville 2002), the Jeans filtering in fossil HII regions after ionizing sources have turned off has not been studied. We argue that it will strongly suppress the mini-halo population, with the following interesting consequences:

- **Impact of Mini-Halo Population on Reioniza-**

<sup>1</sup> For the purposes of this paper, a mini-halo is defined as any halo with  $T_{\text{vir}} < 10^4\text{K}$  which cannot cool via atomic line cooling.

**tion.** Since the recombination time is shorter than the Hubble time at high redshift,  $t_{rec} \ll t_H$ , and the ionizing sources, expected to be massive stars, have short lifetimes,  $t_{MS} \sim 3 \times 10^6 \text{yr} \ll t_H$ , many generations of star formation are required to keep a given patch of the IGM ionized. However, once the first generation of stars born in mini-halos dies out, subsequent generations will not be able to form in mini-halos in a previously reionized patch of IGM, even after the patch cools and recombines. This effect inevitably produces a non-monotonic reionization history with an early peak of partial reionization, followed by recombination and eventual full reionization. This is qualitatively similar to the reionization history derived by Cen (2003) and Wyithe & Loeb (2003), although the physical reason for the non-monotonic evolution in the present work is different (entropy injection, rather than a pop III to pop II transition caused by a universal metallicity increase). Regardless of the extent of UV feedback effects on  $\text{H}_2$  production and cooling, the majority of stars which reionized the universe were hosted by more massive halos able to survive Jeans mass filtering,  $T_{vir} > \text{few} \times 10^4 \text{K}$ .

- **Photon Budget for Reionization.** Dense gas that collects in mini-halos can form a considerable sink of ionizing photons by boosting the overall effective gas clumping factor  $C_{II} = \langle n_e^2 \rangle / \langle n_e \rangle^2$  (Haiman, Abel & Madau 2001; Barkana & Loeb 2002; Shapiro et al 2003). The clumping factor  $C_{II}$  increases rapidly at low redshift as structure formation progresses; thus, despite the higher mean gas density  $n \propto (1+z)^3$  at high redshift, the recombination time  $t_{rec} = 1/(\alpha n_e C_{II})$  does not evolve strongly from  $z = 10-20$ . However, if the universe is filled up with fossil HII regions at high redshift, the photon budgets required to subsequently ionize it and to keep it ionized are much lower, since gas clumping in mini-halos is strongly suppressed.

- **Source Clustering.** Since preheating boosts the threshold mass required for efficient gas cooling and star formation, it increases the mean bias of the early proto-galaxy population by a factor of a few (e.g., see figure 2 of Oh, Cooray & Kamionkowski (2003)). This is likely to increase the clustering amplitude of background fluctuations due to these faint unresolved early proto-galaxies, such as: the free-free background due to ionized halos (Oh 1999; Oh & Mack 2003), Sunyaev-Zeldovich fluctuations due to high redshift HII regions and supernovae winds (Knox et al 1999; Oh, Cooray & Kamionkowski 2003; Santos 2003), and the IR background due to stellar emission (Santos, Bromm & Kamionkowski 2002; Magliocchetti, Salvaterra & Ferrara 2003; Haiman, Spergel & Turner 2003). The increase in clustering bias boosts the amplitude of rms fluctuations by a factor of several. This may be necessary, for instance, if thermal SZ fluctuations from high-redshift supernovae are to account for the small-scale CMB anisotropies observed by BIMA and CBI (Oh, Cooray & Kamionkowski 2003).

- **Star Formation History/Metallicity/IMF.** Initially, each mini-halo is expected to harbor a single massive, metal-free star (no fragmentation is seen in numerical simulations by Abel et al. 2000 and Bromm et al. 2002). Because of the preheating, no further mini-halos can form in the entire comoving volume reionized by this mini-halo. As

a result, the first generation of stars is expected to form as a population of single, isolated stars. Star formation ensues again only once more massive halos with deeper potential wells aggregate. These rare, high density peaks are likely to coincide with the highly biased regions where the first isolated stars had already formed. At the time of the formation of deeper potential wells, such sites are inevitably already polluted with metals, unless the first stars collapsed directly to black holes without associated metal production. As a result, the transition from pop III to pop II (metal free to normal) stellar populations is associated with halo mass scale. This is in contrast to scenarios (Cen 2003; Wyithe & Loeb 2003) where star formation can continually proceed in lower density peaks, which are far from the initial sites of star formation and still contain relatively pristine gas (allowing metal-free star formation to continue to relatively low redshifts). Given the factor of  $\sim 10-20$  difference in the ionizing photon production efficiency per unit mass between Pop III and Pop II stars (Tumlinson & Shull 2000; Bromm, Kudritzki & Loeb 2001; Schaerer 2002), this will have important consequences for the redshift evolution and topology of reionization.

- **21cm Observations.** It has been suggested that mini-halos will be observable at the redshifted 21cm line frequency both in emission (Iliev et al 2002a; Iliev et al 2002b), and absorption (Furlanetto & Loeb 2002). If mini-halo formation is strongly suppressed, these two windows on small-scale structure during the cosmological Dark Ages will disappear. 21cm observations of mini-halos therefore provide an interesting probe of the topology of fossil HII regions: if mini-halos are seen, that comoving patch of the IGM has *never* been ionized. This is complementary to other observations such as Gunn-Peterson absorption, which only probe the instantaneous ionization state.

The rest of this paper is organized as follows. In §2, we compute the “entropy floor” due to early mini-halos. In §3, we calculate the effects of this entropy floor on the gas density profile in mini-halos. In §4, we discuss and quantify several important effects of this entropy floor for reionization, and in §5 we explicitly calculate the effect on the reionization history. We summarize our findings and discuss their implications in §6. Throughout this paper, we adopt the background cosmological parameters as measured by the *WMAP* experiment (Spergel et al. 2003, Tables 1 and 2),  $\Omega_m = 0.29$ ,  $\Omega_\Lambda = 0.71$ ,  $\Omega_b = 0.047$ ,  $h = 0.72$  and an initial matter power spectrum  $P(k) \propto k^n$  with  $n = 0.99$  and normalization  $\sigma_8 = 0.9$ .

## 2 ENTROPY FLOOR DUE TO EARLY REIONIZATION

### 2.1 Entropy floor in Fossil HII regions

Early reionization introduces an ‘entropy floor’ in the intergalactic medium which impedes gas accretion and cooling in halos with  $T_{vir} < 10^4 \text{K}$  which cannot excite atomic cooling. Early reionization even introduces Jeans smoothing effects in halos with  $T_{vir} > 10^4 \text{K}$ , since the strength of the accretion

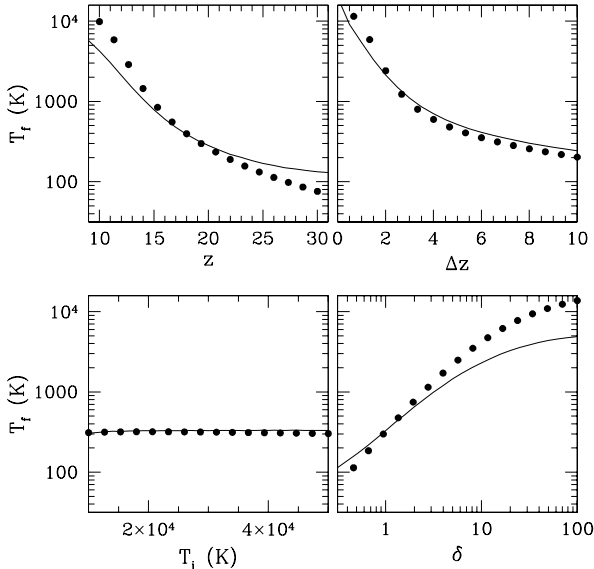


**Figure 1.** The parameter dependence of the final temperature of a parcel of isochorically cooling gas. The solid lines indicate the results from the full non-equilibrium chemistry code, while the points indicate the approximate analytic solution from equations 33 and 35, which is in excellent agreement. Our fiducial patch has an initial temperature  $T_i = 20,000\text{K}$ , cools at  $z = 19$ , for a time interval  $t = 0.6t_H(z = 19) = 1.9 \times 10^8\text{yr}$  (corresponding to roughly  $\delta z \approx 7$ ), and lies at an overdensity  $\delta = 1$ . The gas cools most effectively at high redshift (when the Compton cooling time is short) and at low overdensity (when it decouples from the CMB at late times). For  $z=19$  and  $\delta = 10$ , (which is perhaps characteristic of gas being accreted onto halos) the gas remains at  $\sim \text{few} \times 10^3\text{K}$ .

shock is weaker in preheated gas, and a deeper potential well is required to collisionally ionize the gas. The overall effect is to introduce a substantial core in the gas density profile. The effect is similar to the presumed preheating of the IGM by galactic winds or AGN outflows at low redshift. There, the finite entropy of the gas introduces a core in group and cluster gas density profiles and is thought to be responsible for the deviation from self-similarity in the observed cluster  $L_X - T_X$  relation (for a recent review, see Rosati, Borgani & Norman (2002)). Entropy is more fundamental than gas temperature in low-redshift clusters and high-redshift mini-halos: in both cases, entropy is conserved, since  $t_{\text{cool}} \gg t_H$ . We exploit this analogy, and deliberately employ language and techniques from the well-studied low redshift case to study high-redshift mini-halos. Here, we calculate the expected level of the ‘entropy floor’ due to early reionization.

Reionization is likely to be a highly stochastic process where sources ionize a patch of the IGM and then fade; the fossil HII region subsequently cools and recombines. What is the final temperature a fossil HII region can cool to? At the high redshifts of interest, Compton cooling off the CMB is by far the dominant source of gas cooling in the low density IGM (e.g., at  $z = 19$  and  $T = 10^4\text{K}$ ,  $t_C \sim 0.1t_{\text{cool}}\delta$ , where  $\delta$  is the gas overdensity, and  $t_{\text{cool}}$  is the atomic cool-

ing timescale). The final gas temperature is therefore determined by the competition between Compton cooling and hydrogen recombination: after the gas recombines, it ‘decouples’ from the CMB, and Compton cooling is no longer efficient. The Compton cooling timescale is independent of density and temperature:

$$t_C = 3m_e c(4x_e \sigma_T a T_{\text{CMB}}^4)^{-1} = 1.4 \times 10^7 \left(\frac{1+z}{20}\right)^{-4} x_e^{-1} \text{yr}, \quad (1)$$

whereas the recombination time

$$t_{\text{rec}} = 3.9 \times 10^7 \left(\frac{1+z}{20}\right)^{-3} \delta^{-1} x_e^{-1} \text{yr} \quad (2)$$

is shorter for higher density gas. Thus, denser gas ‘decouples’ from the CMB earlier and freezes out at *higher* temperatures. For the redshifts of interest,  $t_{\text{rec}}(\delta = 1) > t_C$ , allowing for substantial cooling below  $\sim 10^4\text{K}$ .

We can study the temperature evolution of a cooling and recombining parcel of gas  $T(t, T_i, \delta, z)$  as a function of time  $t$  (or redshift interval  $\delta z$ ), initial temperature  $T_i$ , gas overdensity  $\delta_i$  and redshift  $z$ . In Figure 2 we show the dependence of the final temperature on these parameters by solving the full set of chemical evolution equations for primordial gas. We neglect  $\text{H}_2$  chemistry as a trace UV flux is sufficient to photodissociate  $\text{H}_2$  at these low IGM densities. Our fiducial patch has an initial temperature  $T_i = 20,000\text{K}$ , cools at  $z = 19$ , for a time interval  $t = 0.6t_H(z = 19)$  (corresponding to roughly  $\delta z \approx 7$ ), and lies at an overdensity  $\delta = 1$ ; each panel shows the dependence on one of the variables holding the others fixed. We do not take into account time-dependent variation of the gas density arising from infall onto non-linear structures or Hubble expansion, which would provide adiabatic heating/cooling of the gas; however the effects of this may be roughly estimated by considering some mean overdensity  $\delta$  of the gas during its evolution. The final temperature is almost independent of  $T_i$ , as long as  $t \gg t_C$  and the gas was initially fully ionized. However, the final temperature declines at higher redshifts and low overdensities  $\delta$ , since  $t_C/t_{\text{rec}} \propto (1+z)^{-1}\delta$ , and the gas cools faster than it recombines.

In Appendix I, we develop an analytic expression for  $T(t, T_i, \delta, z)$  taking into account only Compton cooling and recombination which is remarkably accurate; it is given by the points in Figure 1. This allows one to estimate the final temperature quickly without evolving the coupled differential equations. It deviates from the true answer significantly only at high overdensity and/or low redshift, when atomic line cooling becomes comparable to Compton cooling. In any case, for metal-free gas, line cooling alone can only cool the gas down to  $\sim 5000\text{K}$ . The only processes which could alter the final entropy of the gas significantly are  $\text{H}_2$  cooling and metal line cooling. These are more efficient than Compton cooling only in regions of high overdensity, in the halo core, and so do not affect the initial entropy floor.

Once cooling becomes ineffective, the gas evolves adiabatically. In accordance with convention, we shall refer to the quantity:

$$K = \frac{T}{n^{2/3}} = 100 \left(\frac{k_B T}{1\text{eV}}\right) \left(\frac{n_e}{10^{-3}\text{cm}^{-3}}\right)^{-2/3} \text{eV cm}^2 \quad (3)$$

as the 'entropy' of the gas, even though it is not strictly the thermodynamic entropy  $S \propto \log(K)$ . This is a useful convention because  $K$  is conserved when the gas evolves adiabatically. Thus, it is conserved during Hubble expansion, as well as during accretion onto halos (provided the accretion shock is weak, gas will be accreted isentropically). In Figure 2, we show the dependence of the final entropy  $K$  on redshift (the dependence on  $T_i, t$  follow simply from Figure 1). The gas has significantly lower entropy at higher redshift, since Compton cooling is more efficient. However, the final entropy at a given redshift depends only weakly on the overdensity  $\delta$ . Denser gas remains at higher temperature, since it recombines faster than it cools, and the combination of higher temperature and higher density roughly cancel  $K \propto T\delta^{-2/3}$ . We can therefore ignore the weak  $\delta$  dependence of  $K$ , and assume that it depends only on  $z$ . *The entropy floor is thus roughly independent of the details of structure formation and gas density distribution.*

It is useful to define a parameter which compares the IGM entropy floor to the entropy generated by gravitational shock heating alone. Let us define the quantity  $\hat{K} \equiv K_{\text{IGM}}/K_o$ , where  $K_o = T_{\text{vir}}/n(r_{\text{vir}})^{2/3}$ , and  $n(r_{\text{vir}}) = (\Omega_b/\Omega_m)\rho_{\text{NFW}}(r_{\text{vir}})/(\mu m_p)$  (and  $\rho_{\text{NFW}}$  is the NFW (Navarro, Frenk & White 1997) dark matter density profile). This is the entropy due to shock heating alone at the virial radius; the justification will become clearer in the ensuing section. As  $\hat{K}$  increases, the Jeans smoothing effects due to finite IGM entropy become increasingly more significant. This parameter  $\hat{K}(K_{\text{IGM}}, T_{\text{vir}}, z)$  will be used extensively in the following sections, and it is useful here to get a sense of what values of  $\hat{K}$  are expected. In Figure 3, we plot  $\hat{K}$  for a  $T_{\text{vir}} = 9000\text{K}$  halo as a function of redshift, using  $K_{\text{IGM}}(z)$  shown in Figure 2. Since  $\hat{K} \propto T_{\text{vir}}^{-1}$ , and a  $T_{\text{vir}} = 9000\text{K}$  halo is about the most massive that would still not experience atomic cooling, the solid line depicts a lower limit on  $\hat{K}$  for all mini-halos. Appropriate values for  $\hat{K}$  for smaller halos can be read off simply from the  $\hat{K} \propto T_{\text{vir}}^{-1}$  scaling. We see that for most halos,  $\hat{K} > 1$ ; although  $K_{\text{IGM}}(z)$  falls at high redshift, this is somewhat offset by the fact that typical potential wells are much shallower, and thus  $K_o$  also falls rapidly (as seen by the dashed lines, which depict  $\hat{K}$  for  $2\sigma$  and  $3\sigma$  fluctuations).

Typical values for  $\hat{K}$  are illustrated further in Figure 4, where we show the mass weighted fraction of mini-halos which have entropy parameters less than a given  $\hat{K}$ , given by:

$$f(< \hat{K}, z) = \frac{\int_{M_J}^{M(\hat{K})} dMM(dn/dM)}{\int_{M_J}^{M_u} dMM(dn/dM)} \quad (4)$$

where  $M(\hat{K})$  is the mass corresponding to  $\hat{K}$  for a given  $K_{\text{IGM}}(z)$ ,  $M_J(z)$  is the cosmological Jeans mass (e.g., see Barkana & Loeb (2002)),  $M_u(z)$  is the mass corresponding to a  $T_{\text{vir}} = 10^4\text{K}$  halo, and  $dn/dM$  is the Press-Schechter mass function. Virtually all halos have  $\hat{K} > 1$  in fossil HII regions at all redshifts of interest ( $z \lesssim 20$ ), and median values of  $\hat{K}$  are much higher. We shall soon see that such halos are subject to very substantial Jeans smoothing effects.

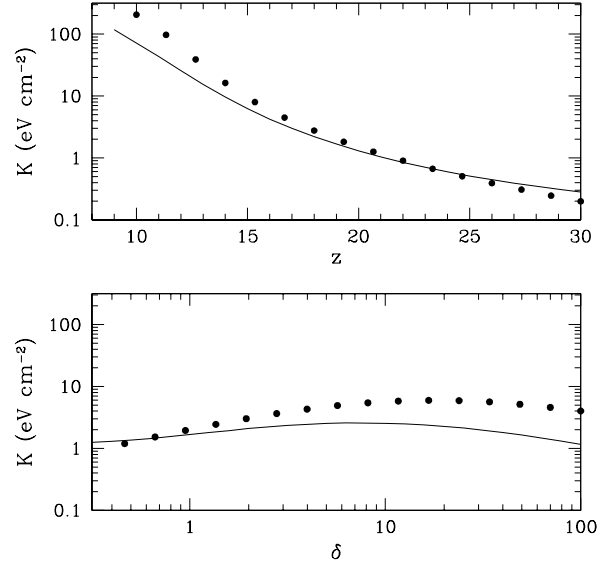


**Figure 2.** Dependence of the final entropy  $K = T/n^{2/3}$  on redshift  $z$  and overdensity  $\delta$ . Points correspond to the analytic solution from equations 33 and 35. As in Figure 1, our fiducial patch has  $T_i = 1$ ,  $\delta = 1$ ,  $z = 19$ ,  $t = 0.5t_H(z = 19)$ . The dependence on  $T_i$  and  $t$  are the same as in Figure 1. The gas retains more entropy at lower redshift, since Compton cooling is less efficient. However, the final entropy shows only a weak dependence on overdensity  $\delta$ : the gas cools out at higher temperatures at higher densities, and the increased temperature and density roughly cancel.

## 2.2 Entropy Floor due to X-rays

Reionization by X-rays (Oh 2001; Venkatesan et al 2001) would produce a warm (few  $\times 100 - 1000\text{K}$ ), weakly ionized IGM with an entropy floor similar to that in fossil HII regions. Such X-rays could arise from supernovae, AGN, or X-ray binaries, or in more exotic models with decaying massive sterile neutrinos (Hansen & Haiman 2003). The universe is optically thick to all photons with energies:

$$E < E_{\text{thick}} = 1.8 \left( \frac{1+z}{15} \right)^{0.5} x_{\text{HI}}^{1/3} \text{keV} \quad (5)$$

where  $x_{\text{HI}}$  is the mean neutral fraction, and we have assumed  $\sigma_\nu \propto \nu^{-3}$ . Thus, *all* energy radiated below  $E_{\text{thick}}$  will be absorbed. The relative efficiency of UV photons and X-rays in setting an entropy floor deserves detailed separate study; here we discuss some salient points. UV photons are an 'energetically extravagant' means of producing an entropy floor. Most of the energy injected by UV photons is lost to recombinations and Compton cooling at high redshift; we see in Figure 1 that the gas typically Compton cools to  $T_{\text{floor}} \sim \text{few} \times 100\text{K}$  at the redshifts of interest. Thus, only  $\sim 10^{-2}$  of the heat injected by UV photons is eventually utilized in setting the entropy floor; all energy expended in heating the gas above  $T_{\text{floor}}$  is 'wasted' (it is dumped into the CMB, where it may eventually be observable as a spectral distortion, Fixsen & Mather 2002). On the other hand, in the weakly ionized gas produced by X-rays, both the re-

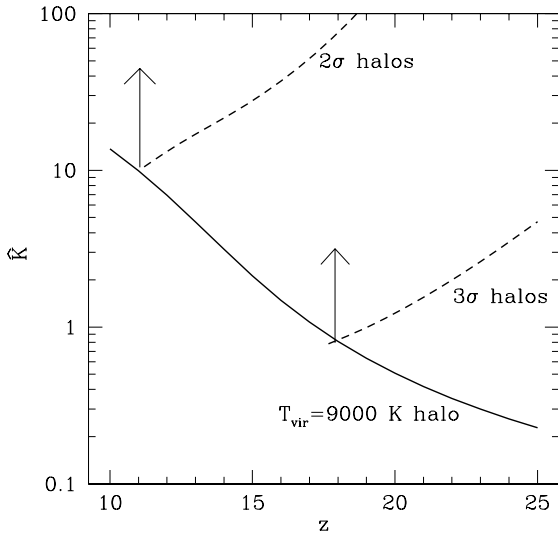


**Figure 3.** The evolution of the dimensionless entropy parameter  $\hat{K} \equiv K_{\text{IGM}}/K_o$  as a function of redshift, assuming the gas cools at the mean IGM density  $\delta = 1$ . Here  $K_o$  is the gas entropy at the virial radius due to shock heating alone, and  $K_{\text{IGM}}$  is the entropy of the fossil HII regions as computed in Figure 2. The solid line describes a  $T_{\text{vir}} = 9000\text{K}$  halo, the most massive in which atomic cooling is still not important. It therefore defines a lower limit on  $\hat{K}$ . The entropy parameter can be simply scaled ( $\hat{K} \propto T_{\text{vir}}^{-1}$ ) for halos with lower virial temperatures. The dashed lines show  $\hat{K}$  for  $2\sigma$  and  $3\sigma$  halos at that redshift; the vast majority of mini-halos have  $\hat{K} > 1$ .

combination time and the Compton cooling time are longer than the Hubble time. In particular,

$$t_C = 1. \left(\frac{x_e}{0.1}\right)^{-1} \left(\frac{1+z}{15}\right)^{-2.5} t_H \quad (6)$$

and almost none of the entropy injected is lost to cooling. Furthermore, a larger fraction of the X-ray energy goes toward heating rather than ionization (in general,  $\text{few} \times 0.1$  of the energy of the hot photo-electron created by an X-ray goes toward heating; this fraction quickly rises toward unity as the medium becomes progressively more ionized (Shull & van Steenberg 1985)). Thus, if  $\epsilon_{\text{bol}}(\text{X-ray})/\epsilon_{\text{bol}}(\text{UV}) \geq 10^{-2}$  (where  $\epsilon_{\text{bol}}$  is the comoving emissivity), X-rays could be comparable or even more effective than UV photons in setting an entropy floor. The relative emissivities of UV and X-rays is unknown, but for supernovae could be as high as (Oh 2001):

$$\frac{\epsilon_{\text{bol}}(\text{X-ray})}{\epsilon_{\text{bol}}(\text{UV})} \approx 0.1 \left(\frac{f_{\text{esc}}}{0.1}\right)^{-1} \left(\frac{f_X}{0.1}\right) \quad (7)$$

where  $f_{\text{esc}}$  is the escape fraction of ionizing UV photons from the host halo, and  $f_X$  is the fraction of supernova explosion energy which goes into soft X-rays, either through inverse Compton scattering of CMB photons by relativistic electrons (Oh 2001), or free-free emission from the hot SN remnant.

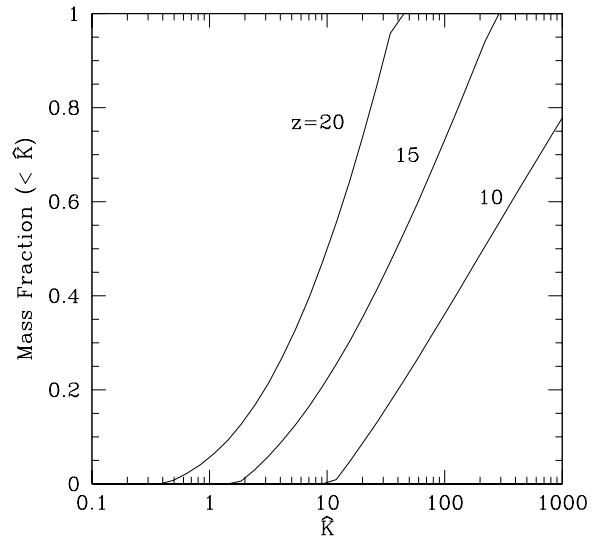


**Figure 4.** The mass weighted fraction of mini-halos which have entropy parameters  $< \hat{K}$ , for  $z = 10, 15, 20$ , assuming  $K_{\text{IGM}}(z)$  shown in Figure 2. Virtually all halos have  $\hat{K} > 1$ , and the median value of  $\hat{K}$  is substantially higher. Thus, the vast majority of halos accrete gas isentropically.

To make a quick estimate, let us (fairly conservatively) assume that  $f_X \sim 3\%$  of the explosion energy of a supernova goes into soft X-rays. Of this,  $f_{\text{heat}} \sim 50\%$  of the energy goes into heating; the rest goes into secondary ionizations and atomic excitations. A supernova releases  $E_Z \sim 0.5\text{MeV}$  in explosion energy per metal baryon, relatively independent of metallicity (a Pop III ‘hypernova’ produces  $\sim 100$  times more energy, but also  $\sim 100$  times more metals than a standard type II SN). X-ray heating thus results in an entropy floor  $K_{\text{IGM}} \approx (f_X E_Z f_{\text{heat}} \bar{Z})/n^{2/3}$ , or:

$$K_{\text{IGM}} \approx 20 \text{ eV cm}^2 \left(\frac{f_X}{0.03}\right) \left(\frac{f_{\text{heat}}}{0.5}\right) \left(\frac{\bar{Z}}{10^{-3} Z_\odot}\right) \left(\frac{1+z}{15}\right)^{-2} \quad (8)$$

where  $\bar{Z}$  is the mean metallicity of the universe. This is comparable to the entropy of fossil HII regions, but has a much larger filling factor, of order unity. A metallicity of  $\bar{Z} \sim 10^{-3} Z_\odot$  corresponds to roughly  $\sim 1$  ionizing photon per baryon in the universe, both for Pop II and Pop III stars. Due to recombinations, the filling factor of ionized regions will be of course considerably less than unity. However, the filling factor of fossil HII regions, which is the relevant quantity, will also be less than unity by a factor  $f_{\text{overlap}}$ , which represents the overlap of HII regions with fossil HII regions which have recombined. Energy spent in reionizing fossil HII regions is ‘wasted’ in terms of establishing an entropy floor. This factor is likely to be large because early galaxy formation is highly biased, and higher mass halos (which can resist feedback effects) will be born in regions already pre-reionized by earlier generations of mini-halos. A fossil HII filling factor of order unity with little overlap

can only be achieved if the formation of mini-halos is highly synchronized (see discussion in section 5).

The mean free path of X-ray photons generally exceeds the mean separation between sources, becoming comparable to the Hubble length for  $\sim 2\text{keV}$  photons. The entire universe is thus exposed to a fairly uniform X-ray background, and the entire IGM acquires a uniform entropy floor, with an amplitude which scales with the amount of star formation, as in equation (8). Even regions far from sites of star formations, which have never been engulfed in an HII region, will be affected. By contrast, in pure UV reionization scenarios, there are large spatial fluctuations in entropy, which depend on the topology of reionization, and the redshift at which a comoving patch was last ionized.

Because of the relative uncertainty of the amplitude of the X-ray background, we use the entropy floor associated with fossil HII regions in the rest of this paper. The mass fraction of affected mini-halos scales with the filling factor of fossil HII regions. This is therefore a minimal estimate; the filling factor could approach unity if X-rays are important.

We now consider the effects of a finite entropy floor on mini-halo gas density profiles.

### 3 GAS DENSITY PROFILES

Once Compton cooling and radiative cooling become inefficient, the gas evolves adiabatically. We can therefore compute static equilibrium density profiles, and see how they change as a function of the entropy floor. The models we construct are in the spirit of Voit et al (2002); Tozzi & Norman (2001); Oh & Benson (2003); Babul et al (2002), which match observations of low-redshift cluster X-ray profiles well.

Naively, one might assume that only gas which remains at temperatures comparable to the virial temperatures of mini-halos would suffer appreciable Jeans smoothing. Since in many cases the IGM can cool down to  $\text{few} \times 100\text{K}$ , one might assume that this level of preheating would have negligible effects on the density profile of gas in mini-halos. This is false: the important quantity is not the temperature but the entropy of the gas. Since gas in the IGM is heated at low density, it has comparatively high entropy. Gas at mean density which is heated to temperatures:

$$T_{\text{IGM}} > 90 \left( \frac{T_{\text{vir}}}{3000\text{K}} \right) \left( \frac{\delta}{200} \right)^{-2/3} \text{K} \quad (9)$$

(where  $\delta$  is the overdensity of the gas in the mini-halo in the absence of preheating) will have entropy in excess of that acquired by gravitational shock heating alone. Its temperature will therefore exceed the virial temperature after infall and adiabatic compression. As the level of preheating increases, gas at progressively larger radii in the halo undergoes Jeans smoothing effects. We now calculate this in detail.

We first construct the default entropy profile of the gas without preheating. We assume that in the absence of heating or cooling processes, the gas distribution traces that of the dark matter, an ansatz which is indeed observed in numerical simulations (e.g., (Frenk et al 1999)) (the dark matter is assumed to follow the NFW (Navarro, Frenk & White

1997) profile). This assumption becomes inaccurate at the very center of the halo, where finite gas pressure causes the gas distribution to be more flattened and less cuspy than the dark matter density distribution. In particular, even in the absence of preheating the IGM has a finite temperature after decoupling from the CMB and cooling adiabatically:  $T_{\text{min}}(z) \approx 2.73(1+z_d)[(1+z)/(1+z_d)]^2$ , where the matter-radiation decoupling redshift  $z_d \approx 150$ . This gives rise to a finite entropy floor:

$$K_{\text{min}} = 4.6 \times 10^{-2} \text{eVcm}^2, \quad (10)$$

independent of redshift. Thus, there will be a finite core in the gas density profile even in the absence of preheating. In regions where gas traces the dark matter, hydrostatic equilibrium gives the entropy profile due to shock heating as:

$$K_{\text{shock}}(r) = \frac{1}{\rho_g(r)^\gamma} \times \left[ \int_{r_{\text{vir}}}^r -\frac{GM(r)\rho_g(r)}{r^2} dr + \frac{\rho_g(r_{\text{vir}})}{\mu m_B} k_B T_{\text{vir}} \cdot (r_{\text{vir}}) \right]. \quad (11)$$

The final entropy profile is therefore  $K(r) = \max[K_{\text{min}}, K_{\text{shock}}(r)]$ . Note that the mean molecular weight is  $\mu = 0.59$  for fully ionized gas and  $\mu = 1.22$  for fully neutral primordial gas; in the paper we are dealing with the case where the ionization fraction is small and therefore use the latter figure. This results in virial temperatures which are higher by a factor  $\sim 2$ .

What is the effect of preheating on the entropy profile? If the infall velocity does not exceed the local sound speed, then the gas is accreted adiabatically and no shock occurs; the gas entropy  $K_{\text{IGM}}$  is therefore conserved. If gas infall is supersonic, then the gas is shocked to the entropy  $K_{\text{shock}}$  computed in equation (11). Tozzi & Norman (2001) found that the transition between the adiabatic accretion and shock heating regime is very sharp. To a very good approximation  $K(M) = \max(K_{\text{shock}}(M), K_{\text{IGM}})$ ; with this new entropy profile we can compute density and temperature profiles. In fact, for most high redshift mini-halos the 'preheating' entropy exceeds the shock entropy even at the virial radius, so the gas mass is accreted isentropically. This occurs when the entropy floor exceeds:

$$K_{\text{IGM}} > 2.3 \text{eV cm}^{-3} \left( \frac{T_{\text{vir}}}{5000\text{K}} \right) \left( \frac{\delta}{50} \right)^{-2/3} \left( \frac{1+z}{20} \right)^{-2}, \quad (12)$$

where the gas overdensity  $\delta \sim 50$  at the virial radius in the absence of preheating is a weak function of the NFW concentration parameter  $c$ . Although  $c$  depends weakly on the collapse redshift, for simplicity we shall assume in this paper that  $c = 5$  for all mini-halos.

We have compared our entropy profiles calculated with equation (11) with the prescription in Tozzi & Norman (2001) (and also adopted by Oh & Benson (2003)). In this method an accretion history for a halo is prescribed via extended Press-Schechter theory; this allows one to compute the strength of the accretion shock and thus the gas entropy (using standard Rankine-Hugoniot jump conditions) for each Lagrangian mass shell. The two methods agree ex-

tremely well; we therefore use equation (11) for both speed and simplicity.

Given an entropy profile, from hydrostatic equilibrium the density profile of the gas is then given by:

$$\rho(r) = \tilde{K}(r)^{-1/\gamma} \times \left[ P(r_{\text{vir}})^{1-\frac{1}{\gamma}} + \frac{\gamma-1}{\gamma} \int_{r_{\text{vir}}}^r -dr' \frac{GM(r')}{r'^2} \tilde{K}(r')^{-1/\gamma} \right]^{1/(\gamma-1)} \quad (13)$$

where  $\tilde{K} \equiv P/\rho^{5/3} = k_B(\mu m_H)^{-5/3} K$ . The temperature profile can then be determined from  $T = \frac{\mu m_H}{k_B} \tilde{K} \rho_{\text{gas}}^{\gamma-1}$ .

The solution of this equation requires a boundary condition which sets the overall normalization, here expressed as  $P(r_{\text{vir}})$ . There is some ambiguity in this choice. The often used boundary condition  $M_g = f_B M_{\text{halo}}$  at  $r = r_{\text{vir}}$  is unphysical as it does not take into account the suppression of accretion due to finite gas entropy. We make the following choice. Let us define  $P_{\text{shock}}(r_{\text{vir}}) \equiv (\Omega_b/\Omega_m)\rho(r_{\text{vir}})/(\mu m_H)k_B T_{\text{vir}}$ , the pressure at the virial radius due to shock heating alone. For  $K_{\text{shock}}(r_{\text{vir}}) > K_{\text{IGM}}$ , the final conditions at the virial radius are not strongly affected by the entropy floor, since the shock boosts the gas onto a new adiabat. We therefore set  $P(r_{\text{vir}}) = P_{\text{shock}}(r_{\text{vir}})$ . The boundary condition must change when  $K_{\text{IGM}} > K_{\text{shock}}(r_{\text{vir}})$ , when accretion takes place isentropically, and the entropy floor is fundamental in determining the gas pressure. In this case,  $P(r_{\text{vir}})$  (which is essentially a constant of integration) is chosen so that  $\rho(r) \rightarrow \bar{\rho}$  as  $r \rightarrow \infty$ . The latter boundary condition implicitly assumes that hydrostatic equilibrium prevails beyond the virial radius. This is questionable, but is arguably reasonable: the gas sound speed  $c_s = (\gamma K_{\text{IGM}} \rho^{\gamma-1})^{1/2}$  in preheated gas is much higher than in cold gas, which is essentially in free-fall. The sound-crossing lengthscale over which hydrostatic equilibrium can be established,  $L_{sc} \approx c_s t_H$ , is:

$$L_{sc} \approx 1 \text{ kpc } h^{-1} \left( \frac{K_{\text{IGM}}}{3 \text{ eV cm}^2} \right)^{1/2} \left( \frac{1+z}{20} \right)^{-0.5} \left( \frac{\delta}{10} \right)^{1/3} \quad (14)$$

which is  $\sim 5$  times larger than the virial radius for a  $\sim 6000K$  halo at the same redshift. Indeed, by definition  $L_{sc} > r_{\text{vir}}$  for Jeans smoothing effects to be important.

Having established the appropriate boundary conditions, we can now compute detailed gas profiles. The entropy, density, pressure and temperature profiles as a function of  $\tilde{r} \equiv r/r_{\text{vir}}$  are shown in Fig 5. These profiles are of course universal and independent of halo mass once  $\tilde{K}$  is set, if the weak dependence of the NFW concentration parameter  $c$  with mass is ignored. As the entropy floor increases, the central pressure and density decline, while the central temperature increases. We see that reasonable values of the entropy floor  $\tilde{K} > 1$  produce dramatic effects on the gas density profile of the halo, smoothing it out considerably.

We now use these density profiles to compute how the accreted gas fraction  $f_g \equiv (M_g/M_{\text{halo}})/(\Omega_b/\Omega_m)$  scales with the entropy parameter  $\tilde{K}$ . This is shown as the dark solid line in Fig 6. Again, because of the self-similarity of the problem, this plot is valid for mini-halos of all virial temperatures at all redshifts, provided  $\tilde{K}$  is appropriately re-scaled. It is reassuring to see that  $f_g$  is continuous at  $\tilde{K} = 1$ , when we switch from one boundary condition to another. This need

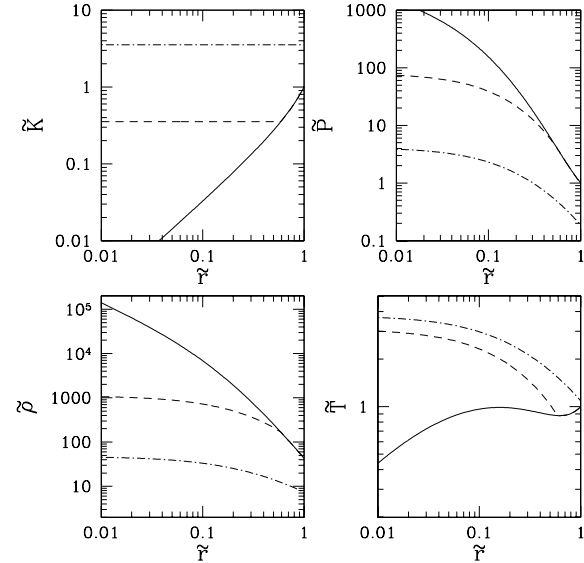


**Figure 5.** The dimensionless entropy  $\tilde{K} = K/K_o$ , pressure  $\tilde{P} = P/P_o$ , temperature  $\tilde{T} = T/T_o$ , and density  $\tilde{\rho} = \rho/\rho_o$ , as a function of radius  $\tilde{r} = r/r_{\text{vir}}$ .  $K_o, P_o, T_o$  are the values of these quantities at  $r_{\text{vir}}$  without preheating, while  $\rho_o = \bar{\rho}_b$ , the mean baryonic density. The entropy profile  $\tilde{K}(\tilde{r})$  uniquely specifies  $\tilde{P}(\tilde{r}), \tilde{T}(\tilde{r}), \tilde{\rho}(\tilde{r})$ , independent of halo mass or redshift.

not have been the case, and gives us confidence that we handle the transition to isentropic accretion correctly. We see that realistic levels of the entropy floor (as computed in §2) causes a substantial depression in gas fractions in mini-halos.

It is interesting to compare our derived gas fractions with other estimates. For the case where  $K_{\text{IGM}} > K_{\text{shock}}(r_{\text{vir}})$ , accretion takes place isentropically. The halo will therefore accrete gas at roughly the adiabatic Bondi accretion rate (e.g., Balogh, Babul & Patton (1999)):

$$\dot{M}_b \approx 1.86\pi\lambda G^2 M_{\text{halo}}^2 \tilde{K}_{\text{IGM}}^{-3/2}. \quad (15)$$

The total accreted gas mass is then roughly  $M_{\text{gas}} \approx \min(f\dot{M}_b t_H, (\Omega_b/\Omega_m)M_{\text{halo}})$ , where  $f$  is some unknown normalization factor which takes into account the fact that the total halo mass is not constant but was lower in the past (and hence, that the gas accretion rate was lower in the past). Another estimate which is a good fit to the results of hydrodynamic simulations is (Gnedin 2000):

$$\bar{M}_b \approx \frac{(\Omega_b/\Omega_m)M_{\text{halo}}}{[1 + (2^{1/3} - 1)M_{1/2}/M_{\text{halo}}]^3}. \quad (16)$$

There is only one free parameter:  $M_{1/2}$ , the mass of the halo in which the gas mass fraction  $f_g = 0.5$ . Gnedin (1999) shows that  $M_{1/2}$  is well approximated by the “filtering mass”  $M_F$ . However,  $M_F$  depends on the unknown thermal history of the IGM. To make a self-consistent comparison, we compute  $M_{1/2}$  with the density profiles computed with our fiducial boundary conditions. Interestingly, we find that  $M_{1/2}$  roughly corresponds to the halo mass when accretion begins to take place isentropically  $\tilde{K} \sim 1$ .

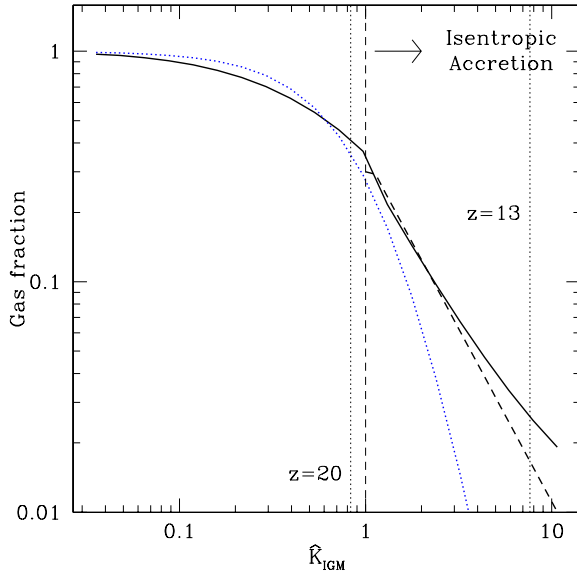


**Figure 6.** The gas fraction within the virial radius  $f_{\text{gas}} = (M_g/M_{\text{halo}})/(\Omega_b/\Omega_m)$  as a function of the entropy parameter  $\hat{K}$ . The solid line indicates our fiducial boundary conditions; the dotted line corresponds to the Gnedin (2000) fit to numerical simulations; while the dashed line corresponds to the Bondi accretion prediction (valid only for isentropic accretion,  $\hat{K} > 1$ ). All three show good agreement. The self-similarity of this problem implies that the computed gas fractions applies to mini-halos of all virial temperatures, provided  $\hat{K}$  is appropriately scaled. For illustrative purposes, appropriate values of  $\hat{K}$  for a mini-halo of  $T_{\text{vir}} = 5000\text{K}$  at  $z = 20, 13$  are shown (see Figure 3).

The results are shown in Figure 6. All three estimates agree well (note that the normalization  $f$  of the Bondi accretion prediction is a free parameter; the plot shown is for  $f = 0.3$ ). The widely used Gnedin (2000) fitting formula predicts even lower gas fractions (and as we will see, clumping factors) at high entropy levels  $\hat{K} \gg 1$ . On the other hand, the slope of the  $f_g(\hat{K})$  relation for our boundary conditions agrees very well with the Bondi accretion prediction in this regime. Our boundary conditions therefore yield fairly conservative estimates of the effects of preheating. Moreover, unlike these other estimates, we are able to compute detailed density profiles, which is crucial for some of our later calculations.

There are two other quantities which are of particular interest when computing density profiles. One is the central density  $\rho_c$ , which affects the ability of mini-halos to form  $\text{H}_2$  in the face of UV photo-dissociation. Another is the gas clumping of the halo, defined as:

$$C_{\text{halo}} = \frac{\langle n^2 \rangle}{\langle n \rangle^2}, \quad (17)$$

where the brackets indicate a volume averaged quantity,

$$\langle X \rangle = \frac{1}{V} \int_0^{r_{\text{vir}}} dr 4\pi r^2 X. \quad (18)$$

Note that  $C_{\text{halo}} \geq 1$  always. The clumping factor  $C_{\text{halo}}$  plays

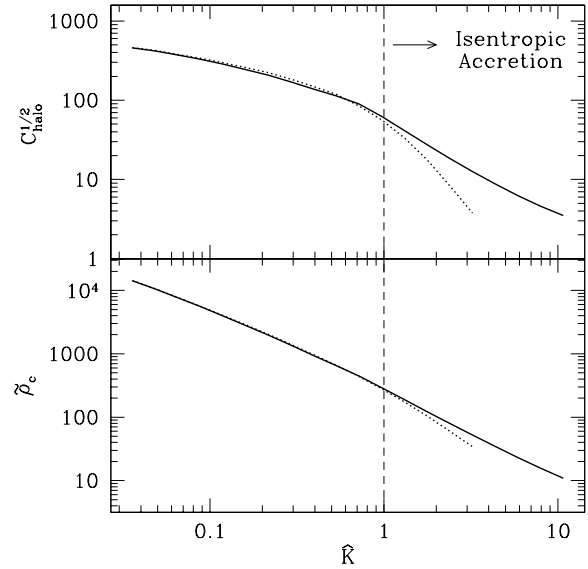


**Figure 7.** The effect of increasing the entropy parameter  $\hat{K}$  on the central gas density  $\bar{\rho}_c = \rho_c/\bar{\rho}$  (bottom panel), and gas clumping  $C_{\text{halo}}^{1/2}$  (top panel), as defined in equation (17). The solid lines correspond to our fiducial boundary conditions, while the dashed lines correspond to adjusting  $P(r_{\text{vir}})$  to reproduce the gas fractions from the Gnedin (2000) fit to numerical simulations (the results for the Bondi accretion prediction are almost identical to the solid curve). Both  $\bar{\rho}_c$  and  $C_{\text{halo}}^{1/2}$  decline rapidly as  $\hat{K}$  increases.

a central role in determining the photon budget required for reionization; we evaluate the global clumping factor in the following section. In Figure 7, we show the effect of increasing the entropy parameter  $\hat{K}$  on the central density and clumping factor. Both decline rapidly with  $\hat{K}$ . We shall use these two results in the following sections.

We now use these gas density profiles to compute global effects of mini-halo suppression.

## 4 GLOBAL EFFECTS OF MINI-HALO SUPPRESSION

### 4.1 Suppression of Collapsed Gas Fraction and Gas Clumping

An entropy floor suppresses the fraction of gas which is bound within mini-halos. As we discuss in §4.4, the mean 21cm emission from mini-halos is directly proportional to this global gas fraction; if it is strongly suppressed the signal will be unobservable. The global collapsed gas fraction is:

$$f_{\text{gas}} = \frac{1}{\rho_b} \int_{M_l}^{M_u} dM \frac{dn}{dM} f_b f_{\text{halo,g}}(\hat{K}) M \quad (19)$$

where  $f_B = \Omega_b/\Omega_m$ ,  $f_{\text{halo,g}}(\hat{K})$  is the halo gas fraction as in Figure 6, and  $\rho_b$  is the comoving baryon density. This is shown in the bottom panel of Figure 9. Curves are shown



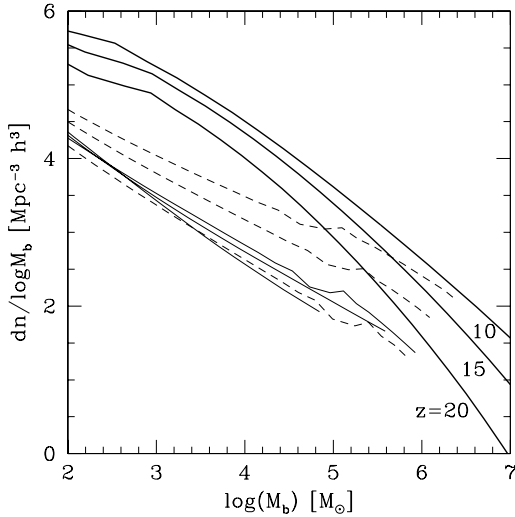


**Figure 8.** The mass function of baryons, as in equation 20, for  $z = 10, 15, 20$ . Dark solid curves show the mass function for  $K_{\text{IGM}} = K_{\text{min}}$ , light solid curves are for redshift-dependent entropy  $K_{\text{IGM}}(z)$  as in the top panel of Figure 2, and dashed curves are for a fixed entropy floor  $K_{\text{IGM}} = 3 \text{ eV cm}^2$ . Note that the baryonic mass function is very similar at all redshifts for  $K_{\text{IGM}}(z)$ . For  $T_{\text{vir}} > 10^4 \text{ K}$ , an entropy floor has no effect on the mass function, which reverts back to the dark solid curves (we do not extend the light solid and dashed curves above the corresponding halo masses).

for no preheating  $K_{\text{IGM}} = K_{\text{min}}$ , fixed values of the entropy floor  $K_{\text{IGM}} = 1, 10 \text{ eV cm}^2$  (which correspond to the IGM settling to some temperature at a given redshift and remaining at constant entropy thereafter), and the redshift dependent entropy  $K_{\text{IGM}}(z)$  shown in the top panel of Fig. 2, which reflects the increasing entropy of gas which Compton cools at late epochs. For realistic values of  $K_{\text{IGM}}$ , the collapsed gas fraction is suppressed by 1–2 orders of magnitude.

It is interesting to plot the effect of preheating on the baryonic mass function. This can be computed simply as:

$$\frac{dN}{dM_b} = \frac{dN}{dM_h} \times \frac{dM_h}{dM_b}. \quad (20)$$

We show this in Fig. 8, at  $z = 10, 15, 20$  for  $K_{\text{IGM}}(z)$  as in the top panel of Fig. 2, and for a fixed entropy floor  $K_{\text{IGM}} = 3 \text{ eV cm}^2$ . As expected, the effect of preheating is most drastic at low masses. Note that the baryonic mass function is very similar at all redshifts for  $K_{\text{IGM}}(z)$ ; this can be also seen in the bottom panel of 9, where the collapsed fraction in mini-halos does not change appreciably with redshift.

Another quantity of great interest is the global gas clumping factor  $C = \langle n^2 \rangle / \langle n \rangle^2$ . Gas clumping shortens the recombination time  $t_{\text{rec}} \approx 1/(anC)$  and thus increases the total number of photons per baryon required to achieve reionization. It is given by:

$$C = (1-f_V)C_{\text{IGM}} + \int_{M_l}^{M_u} \left( \frac{t_{\text{evap}}}{t_H} \right) C_{\text{halo}}(\hat{K}) \frac{dn}{dM} V_{\text{halo}} dM \quad (21)$$

where  $f_V$  is the collapsed fraction by volume of mini-halos,  $C_{\text{IGM}} \approx 1$  is the clumping factor of the IGM,  $C_{\text{halo}}(\hat{K})$  is the halo clumping factor as calculated in the previous section and shown in the top panel of Figure 7, and  $V_{\text{halo}} = (4\pi/3)r_{\text{vir}}^3$  is the volume of a mini-halo. The factor  $(t_{\text{evap}}/t_H)$  deserves some explanation. Mini-halos only contribute to recombinations when they are photoionized. However, once they are exposed to ionizing radiation, they will be evaporated, essentially in the sound crossing time of photoionized gas (Shapiro, Raga & Mellema 1998; Barkana & Loeb 1999). As in Haiman, Abel & Madau (2001), we therefore set the evaporation time  $t_{\text{evap}} = r_{\text{vir}}/(10 \text{ km s}^{-1})$ , and weight the halo clumping factor by the duty cycle  $t_{\text{evap}}/t_H$ .

The clumping factor in equation 21 is a lower limit to the total gas clumping; there will be an additional contribution from larger scales as well. However, the clumping due to minihalos is dominant at the high redshifts of interests.

Our result is shown in the top panel of Figure 9. For the no entropy floor  $K_{\text{IGM}} = K_{\text{min}}$  case (top curve), gas clumping is much lower at high redshift, since fewer mini-halos have collapsed. Once a patch of IGM is reionized early at high redshift, then an entropy floor is established and subsequent gas clumping is suppressed. Thus, early star formation *reduces* the total photon budget required to achieve full reionization. We see that gas clumping is reduced by an order of magnitude even for the low entropy levels  $\sim 1 \text{ eV cm}^2$  associated with reionization at high redshift  $z \sim 20$ . For the redshift-dependent entropy  $K_{\text{IGM}}(z)$  shown in the top panel of Figure 3, mini-halo clumping is strongly suppressed, and  $C \approx 1$ .

## 4.2 Suppression of H<sub>2</sub> formation

H<sub>2</sub> formation and cooling in mini-halos will be suppressed relative to the no preheating case. This is because the finite entropy of the gas allows it to resist compression; thus, the gas is at considerably lower density. Collisional processes with cooling times  $t_{\text{cool}} \propto 1/n$  will be suppressed relative to radiative processes which photo-dissociate H<sub>2</sub>. It has been recognized that gas profiles should have a central core rather than a cusp (e.g., Shapiro, Iliev & Raga (1999)) and that lower central densities will affect H<sub>2</sub> chemistry (Haiman, Rees & Loeb 1996; Tegmark et al 1997). However, the fact that preheating can produce a much larger, lower density core than hitherto considered, and the subsequent implications for H<sub>2</sub> formation and cooling, has not been explored.

It has been shown that H<sub>2</sub> formation is enhanced in fossil HII regions due to increased electron fraction there (Ricotti, Gnedin & Shull 2002). Although H<sub>2</sub> formation is very slow in the low density IGM, a high initial electron abundance will persist when weakly ionized gas is accreted onto non-linear structures, and aid H<sub>2</sub> formation at that point (Oh 2000). We can conservatively take into account the H<sub>2</sub> enhancement by assuming the maximum initial abundance of H<sub>2</sub>,  $x_{\text{H}_2} \sim 10^{-3}$ ; this hard upper limit is independent of density or ionization fraction and is due to ‘freeze-out’

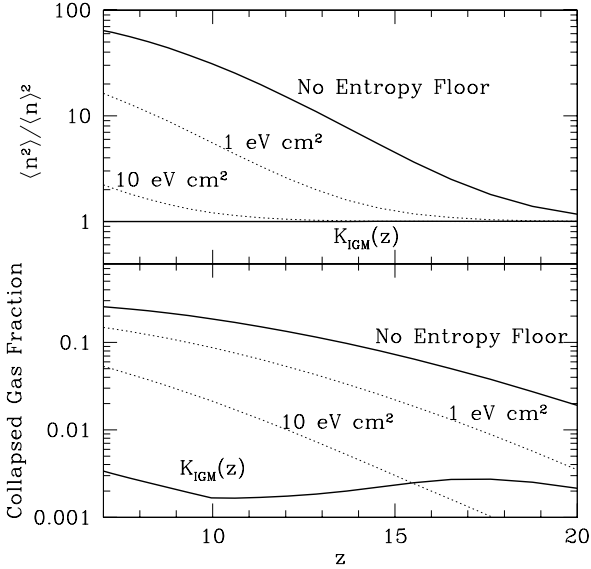


**Figure 9.** The evolution of the collapsed gas fraction in mini-halos (*lower panel*) and the gas clumping factor (*upper panel*) with redshift. The results are shown for no preheating (with  $K_{\text{IGM}} = K_{\text{min}}$ ), as well as constant values of entropy  $K_{\text{IGM}} = 1, 10 \text{ eV cm}^2$  and the redshift-dependent entropy  $K_{\text{IGM}}(z)$  shown in the top panel of Figure 2. Both the global gas fraction in mini-halos and gas clumping are strongly suppressed for realistic values of the entropy floor. In particular,  $C \rightarrow 1$  for realistic values of  $K_{\text{IGM}}$ , greatly reducing the photon budget required for reionization.

(Oh & Haiman (2002), hereafter OH02). The  $\text{H}_2$  abundance can only exceed this if three-body processes are important, which only takes place at very high density  $n > 10^8 \text{ cm}^{-3}$ .

In OH02, we showed that the minimum temperature  $T_{\text{min}}$  a parcel of gas can cool to depends almost exclusively on  $t_{\text{cool}}/t_{\text{diss}} \propto J_{\text{UV}}/n$  (see Figure 6 of OH02). This scaling behavior is only broken when the gas approaches high densities  $n > 10^4 \text{ cm}^{-3}$  (at this point, the cooling time becomes independent of density and  $t_{\text{cool}}/t_{\text{diss}} \propto J_{\text{UV}}$ ). However, the latter regime is never reached in pre-heated gas, which is at much lower densities ( $n \sim 10^4 \text{ cm}^{-3}$  corresponds to  $\delta \sim 6 \times 10^6$  at  $z = 19$ ). In subsequent discussion, we shall assume the dependence of  $T_{\text{min}}$  on  $J_{\text{UV}}/n$  shown in Figure 6 of OH02.

Thus, in the presence of a radiation field  $J_{\text{UV}}$ , the gas must be at a minimum density  $n_{\text{crit}}$  to cool down to a temperature  $T_{\text{min}}$ . We have already calculated the maximum central density  $n_c$  of gas in a halo given an entropy parameter  $\hat{K}$ , as in Figure 7. If the central density is less than the critical density,  $n_c < n_{\text{crit}}$ , then *none* of the gas in the halo can cool down to  $T_{\text{min}}$ . For a given entropy parameter  $\hat{K}$ , there is therefore a minimum radiation field  $J_{\text{UV}}$  above which no gas can cool down to  $T_{\text{min}}$ . We plot this in the top panel of Figure 10. This plot is valid for all halos at all redshifts provided  $\hat{K}$  and  $J_{\text{UV}}$  are both rescaled appropriately (note that since  $n \propto (1+z)^3$ , to keep  $J_{\text{UV}}/n$  constant,  $J_{\text{UV}} \propto (1+z)^3$ ). To get a sense of typical val-

ues of  $J_{\text{UV}}$ , the radiation field corresponding to  $n_\gamma$  ionizing photons per baryon in the universe is  $J_{\text{UV}} \approx \frac{h_P c}{4\pi} n_\gamma n_b (1+z)^3 / 10^{-21} \text{ erg s}^{-1} \text{ cm}^{-2} \text{ Hz}^{-1} \text{ sr}^{-1} \approx 10 n_\gamma \left(\frac{1+z}{16}\right)^3$  (where  $n_b$  is the comoving baryon number density, and  $h_P$  is the Planck constant).

We see that an entropy floor greatly reduces the radiation field required to prevent gas cooling. For reasonable values of  $\hat{K}$ , the reduction can be as much as four orders of magnitude. Thus, even if there is only a very weak radiation field, in the presence of an entropy floor effective  $\text{H}_2$  cooling and star formation will be quenched. Note also that the cooling time exceeds the Hubble time for large values of  $\hat{K}$ . This regime is reached only when gas densities are so low that even a very weak radiation field can dissociate  $\text{H}_2$ :  $t_{\text{cool}} \sim t_{\text{diss}} \sim 2 \times 10^8 (J_{\text{UV}}/10^{-4})^{-1} \text{ yr}$ .

Without an entropy floor, the density profiles of mini-halos at a given redshift are self-similar; thus, roughly comparable fractions of their gas can cool down to  $T_{\text{min}}$  and will be available as fuel for star formation. In the presence of an entropy floor, the fraction of gas with  $n > n_{\text{crit}}$  is greatly reduced, and much less gas can cool. Moreover, the self-similarity is broken: shallower potential wells (which have higher  $\hat{K}$ ) are more strongly affected by an entropy floor, and their central gas densities are much lower. Using our halo density profiles, we can calculate the fraction of gas above the critical density,  $f_{\text{gas}} = M_b(> n_{\text{crit}}) / [(\Omega_b/\Omega_m) M_{\text{halo}}]$ . We plot this in the lower panel of Fig 10. At some critical value of  $\hat{K}$ , the fraction of gas which can cool plummets dramatically. This value of  $\hat{K}$  corresponds roughly to when the low density core falls below the critical density.

Note that we assume static rather than evolving density profiles. In reality, as gas cools, densities should increase as the gas loses pressure support, making the gas more resistant to  $\text{H}_2$  photo-dissociation (Machacek et al. 2001). However, the dynamical time  $t_{\text{dyn}} \approx 10^8 (n/1 \text{ cm}^{-3})^{-1/2} \text{ yr}$  is typically much longer than the photo-dissociation time  $t_{\text{diss}} \approx 2 \times 10^4 J_{\text{UV}}^{-1} f_{\text{shield}}^{-1} \text{ yr}$  (where the factor  $f_{\text{shield}}$  takes into account self-shielding; see discussion in section 4.2.3 of OH02, and references therein). So our use of the initial density profile to estimate timescales should be approximately valid.

We can also compute the critical radiation field required to suppress  $\text{H}_2$  cooling down to some temperature  $T$  as a function of redshift. We plot this in Fig. 11 for a  $T_{\text{vir}} = 8000 \text{ K}$  halo; such a halo represents an upper mass limit to the mini-halo population. Smaller halos, which have lower central densities for a given entropy floor, will require a weaker radiation field for  $\text{H}_2$  cooling to be suppressed. This is shown for four different entropy floors:  $K_{\text{IGM}}(z)$  as shown in Fig. 2, no preheating  $K_{\text{IGM}} = K_{\text{min}}$ , and fixed entropy floors  $K_{\text{IGM}} = 1, 10 \text{ eV cm}^2$ . Gas cooling in fossil  $\text{H}_2$  regions is very easily suppressed; the radiation field required is 2-4 orders of magnitude lower than required in the no preheating case.

One possible caveat is that since fossils are likely to be metal-enriched, gas cooling is dominated by metal line cooling, rather than  $\text{H}_2$  cooling. We argue that this is unlikely, for two reasons: 1) Metal line cooling only dominates  $\text{H}_2$  cooling above a critical metallicity  $Z > 10^{-3} Z_\odot$  (Bromm et al 2001; Hellsten & Lin 1997). This level of metal enrich-

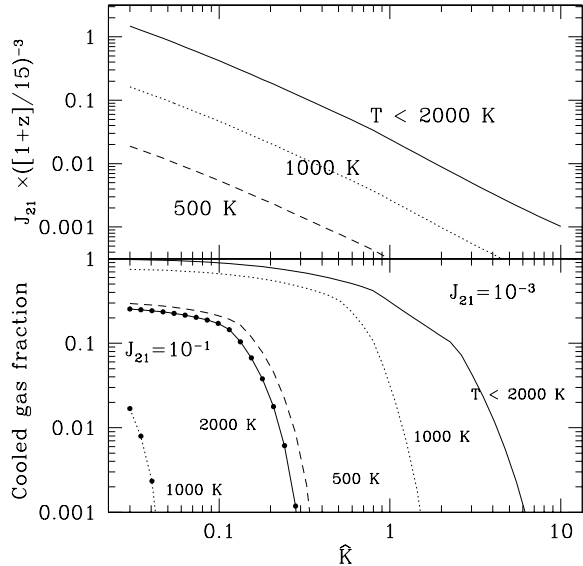


**Figure 10.** *Top panel:* The critical radiation field  $J_{UV}$  required to suppress gas cooling below some temperature  $T$ , as a function of entropy parameter  $\hat{K}$ . An entropy floor greatly reduces the radiation field required to photo-dissociate  $H_2$ , by several orders of magnitude. Note that  $J_{UV} \propto (1+z)^3$ ; the curves shown are for a halo at  $z = 14$ . *Bottom panel:* The fraction of gas in a halo able to cool below temperature  $T$ , for  $J_{UV} = 10^{-3}$  (lines), and  $J_{UV} = 10^{-1}$  (dots connected by lines), at  $z = 14$ . Beyond a critical value of  $\hat{K}$ , the cooled gas fraction plummets dramatically.

ment corresponds to  $\sim 1f_Z^{-1}$  ionizing photon per baryon in the universe (where  $f_Z$  is the volume filling factor of metals). Thus, metal line cooling becomes significant only at late times. 2) After an ionizing source turns off and explodes as a supernova, the metal-polluted region is much smaller than the fossil HII region (Madau, Ferrara & Rees 2001). Most of the volume is therefore still of pristine composition, and undergoes the entropy floor suppression we have described. The metal-polluted region lies close to the high density peak where the very first stars formed, where in any case, more massive halos  $T_{vir} > 10^4 K$  will collapse. To summarize: metal line cooling is therefore unlikely to spoil our assumption of adiabaticity in most of the volume of the fossil HII region. The exception is at the most highly biased density peaks, where metals can be thought of as effectively increasing the star formation efficiency.

The net result is that entropy injection greatly boosts the negative feedback from early star formation: the entropy floor in reionized regions results in low density cores in the center of halos, in which  $H_2$  is easily photo-dissociated by a weak external UV radiation field.

### 4.3 Negative Feedback from X-rays

It is often argued that X-rays boost  $H_2$  production and cooling in mini-halos, by penetrating deep into the dense core and increasing the free electron fraction, which is critical for gas phase  $H_2$  production. Thus, X-rays are thought to exert

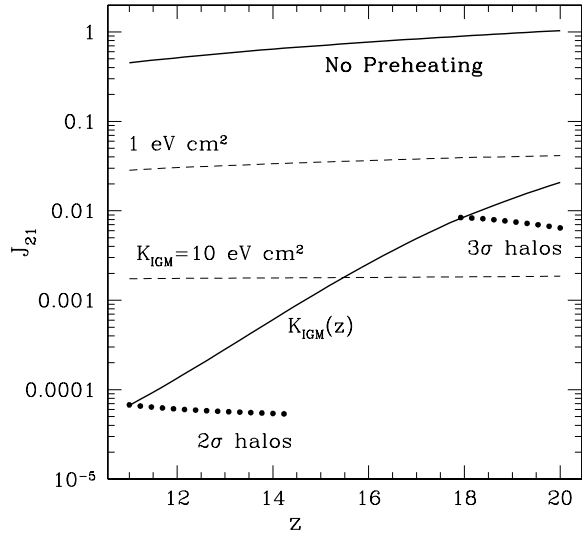


**Figure 11.** The critical radiation field  $J_{UV}$  required to suppress gas cooling below  $T = 1000K$ , as a function of redshift  $z$ . The curves are shown for a  $T_{vir} = 8000K$  halo, which is an upper limit in mass to the mini-halo population: smaller mini-halos will require a weaker radiation field for cooling to be suppressed. The curves are shown for four different entropy floors: no preheating  $K_{IGM} = K_{min}$ , an evolving entropy  $K_{IGM}(z)$  as shown in Fig. 2, and fixed entropy floors  $K_{IGM} = 1, 10 eV cm^2$ . Points are also shown for  $2\sigma$  and  $3\sigma$  halos at each redshift, assuming  $K_{IGM}(z)$  (the points end when  $T_{vir} < 1000K$  and  $T_{vir} > 8000K$  respectively). Typical entropy floors at each redshift reduce the critical radiation field required for  $H_2$  suppression by 2–4 orders of magnitude, compared to the no preheating case.

a positive feedback effect, counter-acting photo-dissociation by UV radiation (Haiman, Rees & Loeb 1996; Haiman, Abel & Rees 2000). We show here by fairly general arguments that X-rays in fact exert a strong *negative* feedback effect, due to the entropy that they inject into the IGM. This prevents gas from compressing to sufficiently high density to produce  $H_2$  and cool efficiently, and far outweighs any positive feedback from increasing the free electron fraction.

For the sake of definiteness, we consider an intrinsic source spectrum of the form

$$\begin{aligned}
 J &= J_{UV} \left( \frac{\nu}{\nu_L} \right)^{-1} \quad h\nu < 13.6eV \\
 &= J_X \left( \frac{\nu}{\nu_L} \right)^{-1} \quad 13.6eV < h\nu < 10keV
 \end{aligned}
 \tag{22}$$

where  $h\nu_L = 13.6eV$  and  $J_{UV}/J_X = f_{break} = 1 - 100$  is the spectral break at the hydrogen Lyman edge; note that  $f_{break} \geq 1$  always. A spectrum of the form  $J_\nu \propto \nu^{-1}$  is characteristic of the mean spectra of quasars (Elvis et al 1994), as well as inverse Compton emission from high-redshift SN (Oh 2001). It is distinctive in that  $\nu J_\nu = const$ , i.e., there is equal power per logarithmic interval (though our arguments can be generalized to other spectra). Note that the actual ionizing spectrum at any given point in the IGM will

be much harder, since photoelectric absorption hardens the spectrum away from the source.

What is the heating associated with this radiation field? As we argued in §2.2 above, all energy in the X-ray radiation field with  $E_L < E < E_{\text{thick}}$  (as defined in §5) will be absorbed by the IGM, since the universe is optically thick at these frequencies. The radiation field may be subdivided into two components. The “mean field” consists of photons with  $E > E_{\text{overlap}}$ , where  $E_{\text{overlap}}$  is defined by:

$$\lambda_{\text{mfp}}(E) > n_{\text{source}}^{-1/3} \quad \text{for } E > E_{\text{overlap}} \quad (23)$$

i.e., photons with  $E > E_{\text{overlap}}$  (typically,  $E_{\text{overlap}} \sim 100\text{eV}$ ) have a mean free path greater than the mean separation between sources, so that a homogeneous ionizing background is established. The “fluctuating field” consists of photons with  $E < E_{\text{overlap}}$ ; this component is dominated by radiation from a single source, and is subject to large Poisson fluctuations. We are interested in the heating due to the ‘mean field’, which can lead to an entropy floor even outside the HII regions of ionizing sources. It is:

$$\dot{E}_{\text{heat}} = f_{\text{heat}} \int_{\nu_{\text{overlap}}}^{\nu_{\text{thick}}} d\nu \epsilon_{\nu} \approx f_{\text{heat}} \frac{4\pi}{l_H} J_X \nu_L \ln \left( \frac{\nu_{\text{thick}}}{\nu_{\text{thin}}} \right) \quad (24)$$

where  $f_{\text{heat}}$  is the fraction of energy of the hot photo-electron created by an X-ray which goes into heating. We have conservatively set  $\epsilon_{\nu} \approx (4\pi J_{\nu})/l_H$ ; this underestimates  $\epsilon_{\nu}$  for a given  $J_{\nu}$ . For the spectrum we have chosen, the result is only logarithmically sensitive to the integration bounds; we set  $\ln(\nu_{\text{thick}}/\nu_{\text{thin}}) \approx 2.3$ . For steeper spectra,  $J_{\nu} \propto \nu^{-\alpha}$  where  $\alpha > 1$ , the lower integration limit becomes important.

Over a Hubble time  $t_H$ , the internal energy density  $U = nk_B T \approx \dot{E}_{\text{heat}} t_H$  of the gas becomes:

$$U \approx f_{\text{heat}} \frac{4\pi}{c} J_X \nu_L \ln \left( \frac{\nu_{\text{thick}}}{\nu_{\text{thin}}} \right) \quad (25)$$

This make sense: since some fraction  $f_{\text{heat}}$  of the radiation field goes directly into heat,  $f_{\text{heat}} 4\pi(\nu J_{\nu}) \approx U c$ . Thus, X-rays will heat the IGM to a temperature:

$$T = 170\text{K} \left( \frac{f_{\text{heat}}}{0.5} \right) \left( \frac{J_X}{10^{-2}} \right) \left( \frac{1+z}{15} \right)^{-3}. \quad (26)$$

There is therefore a direct relation between the X-ray radiation field and the entropy floor:

$$K_{\text{IGM}} = 1.9\text{eV cm}^2 \left( \frac{f_{\text{heat}}}{0.5} \right) \left( \frac{J_X}{10^{-2}} \right) \left( \frac{1+z}{15} \right)^{-5}. \quad (27)$$

As we argued in §2.2 above, the IGM evolves adiabatically for  $x_e < 0.1[(1+z)/15]^{2.5}$ . What level of the radiation field does this correspond to? For  $x_e \leq 0.1$ , about  $f_{\text{ion}} \sim 1/3$  of the injected energy goes toward performing ionizations; the number of photo-ionizations is simply  $E_{\text{photon}}/(37\text{eV})$ . Thus, we obtain:

$$x_e = 2.3 \times 10^{-4} \left( \frac{f_{\text{ion}}}{0.3} \right) \left( \frac{J_X}{10^{-2}} \right) \quad (28)$$

and so for  $J_X < 5$ , the IGM evolves adiabatically (note also that since  $t_{\text{rec}} \approx 10t_H(x_e/10^{-3})^{-1}(T/100\text{K})^{-0.7}([1+z]/15)^{-1.5}$ , we can ignore recombinations).

Given the entropy floor from equation 27, we can now

calculate density profiles of halos. In particular, we can calculate the maximum central density of a halo from the entropy floor induced by a given X-ray background. As before, from the central density of a halo we can calculate the critical level of the LW flux  $J_{\text{UV}}$  required to suppress  $\text{H}_2$  cooling down to some temperature  $T_{\text{min}}$ . This critical flux is shown as a function of  $f_X = J_X/J_{\text{UV}}$  in Fig 12, for a halo of  $T_{\text{vir}} = 5000\text{K}$  at  $z = 19$ . The curves may be simply rescaled for halos of different mass at different redshifts by translating the x-axis:  $f_X \propto T_{\text{vir}}(1+z)^5$ . The effect of X-rays increases for less massive halos (which are less able to withstand an entropy floor) at lower redshifts (when gas densities are lower). Also shown are the maximum value of the X-ray background  $f_X \approx 1$  for the hardest sources, as well as the typical minimum value of the X-ray background required for positive feedback to be effective  $f_X \approx 0.1$  (Haiman, Abel & Rees 2000). The shaded region therefore denotes the X-ray fluxes thought to produce positive feedback effects. We see for these large values of the X-ray background, X-rays *cannot* exert a positive feedback effect. The required X-ray background is so large that it would produce an unacceptably large entropy floor, which prevents the formation of dense regions where  $\text{H}_2$  can withstand photodissociation. Instead, X-rays produce an over-all negative feedback effect. In fact, values of  $f_X \approx 0.1 - 1$  reduce by almost two orders of magnitude the value of the UV background required to photo-dissociate  $\text{H}_2$  and prevent it from cooling down to low temperatures.

The only way of circumventing these difficulties is if X-rays turn on suddenly at some epoch. Halos which have already collapsed will be unaffected by the entropy floor, but will undergo the usual positive feedback from X-rays. However, the subsequent generation of mini-halos will be suppressed by the entropy floor.

#### 4.4 21cm Observational Signatures

At present, the only observational probes proposed for small-scale structure at high redshift such as mini-halos are 21cm observations with future radio telescopes such as the Square Kilometer Array (SKA)<sup>2</sup> and the Low Frequency Array (LOFAR)<sup>3</sup>. It has been proposed that mini-halos could be detected statistically in emission (Iliev et al 2002a; Iliev et al 2002b) and individually in absorption along the line of sight to a high-redshift radio source (Furlanetto & Loeb 2002). If an entropy floor exists, such signatures will be strongly suppressed. 21cm signatures of mini-halos therefore provide an interesting indirect probe of reionization history: if mini-halos *are* detected in large numbers at a given redshift, it would imply that the filling factor of fossil HII regions is still small at that epoch. In particular, a comoving patch where mini-halos are seen has likely never been ionized before (which is a much stronger constraint than merely being neutral at the observed epoch). This could prove a very useful probe of the topology of reionization.

<sup>2</sup> see <http://www.nfra.nl/skai>

<sup>3</sup> see <http://www.astron.nl/lofar>

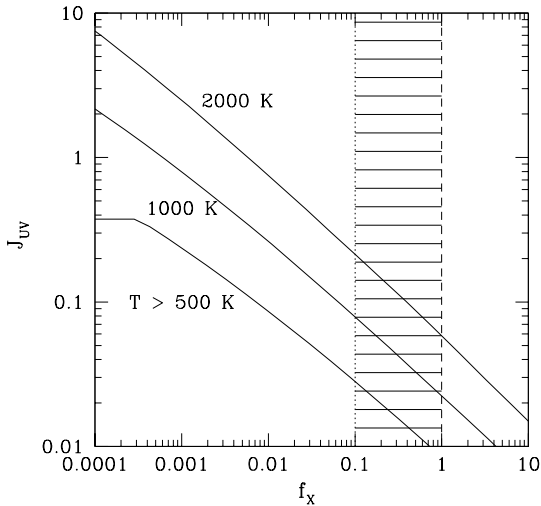


**Figure 12.** The UV background  $J_{UV}$  required to suppress cooling down to some temperature  $T_{\min}$ , as a function of  $f_X = J_X/J_{UV}$ . The curves plotted are for a  $T_{\text{vir}} = 5000\text{K}$  halo at  $z = 19$ ; the results may be rescaled to other halos by rescaling the x-axis:  $f_X \propto T_{\text{vir}}(1+z)^5$ . Also shown as dashed and dotted lines are the maximum value of  $f_X \approx 1$  in the hardest sources, and the minimum typical value of  $f_X \approx 0.1$  required for X-rays to exert a positive feedback effect; the shaded region therefore shows the possible region whereby X-rays were assumed exert a positive feedback effect. Instead, we see that such a strong X-ray background exerts a *negative* feedback effect. By inducing a low density core in the halo, an X-ray background in the required zone reduces by 1–2 orders of magnitude the minimum UV flux required to suppress cooling, compared to the case where  $f_X \rightarrow 0$ .

Mini-halos are too faint to be seen individually in emission, and can only be detected statistically through brightness temperature fluctuations. Provided  $T_S \gg T_{\text{CMB}}$  (where  $T_S$  is the spin temperature), the 21cm flux  $S$  is independent of the spin temperature, and depends only on the HI mass,  $S \propto M_{\text{HI}}$ . Thus,  $S(\text{halos})/S(\text{IGM})$  is simply equal to the collapsed gas mass fraction in mini-halos, which is always less than unity. The mini-halo signal is much smaller if an entropy floor exists, since the collapsed gas fraction declines rapidly: the bottom panel of Figure 9 can simply be read off as  $S(\text{halos})/S(\text{IGM})$ . Thus, the IGM dominates 21cm emission. Mini-halos dominate only when: (i) the IGM spin temperature has not yet decoupled from the CMB (the critical thermalization radiation field  $J_{21}$  such that  $T_S \rightarrow T_\alpha \approx T_K$ , where  $T_\alpha$  is the color temperature of the radiation field, is  $J_{21} \approx 5([1+z]/10)$  (Madau, Meislin & Rees 1997)) (ii) the filling factor of fossil HII regions is small. The high *WMAP* optical depth, which implies significant reionization at high redshift, pushes the latter constraint to high redshift and thus low radio frequencies  $\nu_{\text{obs}} = 93([1+z]/15)\text{MHz}$ , making this a very challenging observation.

We now turn to absorption signatures. How does the

mini-halo 21cm absorption signature scale with the IGM entropy? The IGM 21cm optical depth is:

$$\tau_\nu \approx 10^{-2} \left( \frac{T_{\text{CMB}}(z)}{T_S} \right) \left( \frac{1+z}{10} \right)^{1/2} x_{\text{HI}}. \quad (29)$$

See Madau, Meislin & Rees (1997) for expressions for the spin temperature  $T_S(J_{21}, n_{\text{HI}}, T_K)$ ; we do not reproduce them here. We use a fit to the results of Allison & Dalgarno (1969) for the collisional coupling coefficient  $C_{10}$  for  $T_K < 1000\text{K}$ , with a  $C_{10} \propto T_K^{-0.33}$  extrapolation for higher temperatures. The mini-halo 21cm optical depth along an impact parameter  $\alpha$  to the halo center is (Furlanetto & Loeb 2002):

$$\tau_{\text{halo}}(\alpha, \nu) = \frac{3h_P c^3 A_{10}}{32\pi k_B \nu_o^2} \int dR \frac{n_{\text{HI}}(r)}{T_s(r) \sqrt{\pi} b(r)} \exp \left[ -\frac{v(\nu)^2}{b^2(r)} \right] \quad (30)$$

where  $A_{10} = 2.85 \times 10^{-15} \text{s}^{-1}$  is the spontaneous emission coefficient,  $b(r)^2 = 2k_B T_K / m_p$  is the gas Doppler parameter,  $r^2 = R^2 + \alpha^2$ , and  $v(\nu) = c(\nu - \nu_o) / \nu_o$ . Unlike Furlanetto & Loeb (2002), we do not attempt to model the velocity field of the infall region, which we ignore; the total observed optical depth is taken to be  $\tau_{\text{tot}} = \tau_{\text{halo}} + \tau_{\text{IGM}}$ . The velocity field in the preheated gas will differ significantly from the Bertschinger self-similar solution they assume, since gas pressure retards accretion; the infall region optical depth will be smaller because of the reduced gas column. Since even in their case the contribution of the infall region to 21cm absorption is small (see their Fig. 2, where the equivalent width drops drastically for  $\alpha > r_{\text{shock}}$ ), our neglect is justified.

In Fig. 13, we show the optical depth as a function of observed frequency, for different levels of the entropy parameter  $\hat{K}$ . The values of  $\hat{K}$  shown correspond to IGM temperatures of  $T_{\text{IGM}} = 70, 700, 7000\text{K}$ ; since fossil HII regions at  $z=10$  cannot significantly cool below 7000K (see Fig. 1), the value of  $\hat{K} = 50$  is most appropriate. We see that the optical depth contribution from mini-halos falls drastically with increasing  $\hat{K}$ . Also shown is the optical depth for  $J_{21} = 10$ . The radiation field drives  $T_S \rightarrow T_K$ , reducing the 21cm optical depth  $\tau \propto T_S^{-1}$ .

Since  $\tau_{\text{IGM}}$  also depends on  $\hat{K}$ , the most relevant quantity for detecting a mini-halo is the observed equivalent width:

$$\langle \Delta\nu \rangle = \frac{2}{1+z_h} \left[ \int_{\nu_o}^{\infty} d\nu (1 - e^{\tau_{\text{tot}}}) - (1 - e^{\tau_{\text{IGM}}}) \right] \quad (31)$$

which measures the 21cm absorption due to the mini-halo in excess of that due to the IGM. It falls rapidly with  $\hat{K}$  and is extremely small for the most likely value of  $\hat{K} = 50$ . Figures 13 and 14 can be compared with Fig. 1 and 2 of Furlanetto & Loeb (2002) (although note that in Fig. 13, we plot  $\tau$  as a function of observed rather than intrinsic frequency). An entropy floor greatly reduces the cross-sectional area over which an observable absorption signal may be detected. If one detects significant mini-halo absorption over a large comoving patch along the line of sight to a radio source, one can place an upper limit on the entropy floor there. This in turn places an upper limit on the high-redshift X-ray background (from equation 8), as well as a lower limit on the

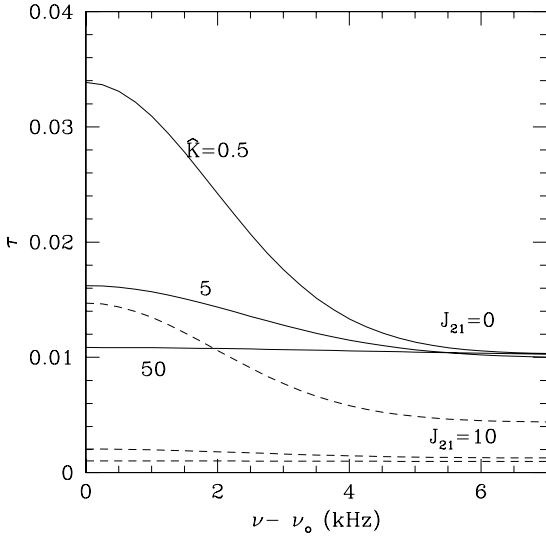


**Figure 13.** Mini-halo optical depth profiles as a function of observed frequency for a  $2 \times 10^6 M_\odot h^{-1}$  halo at  $z = 10$ , all for impact parameters of  $\alpha = 0.3r_{\text{vir}}$ . The values of  $\hat{K} = 0.5, 5, 50$  shown correspond to IGM temperatures of  $T_{\text{IGM}} = 70, 700, 7000\text{K}$ ; since fossil HII regions at  $z=10$  cannot significantly cool below  $7000\text{K}$ , the value of  $\hat{K} = 50$  is most appropriate. Solid lines correspond to  $J_{21} = 0$ ; dashed lines correspond to  $J_{21} = 10$ . The entropy floor makes the mini-halo contribution to the 21cm absorption undetectable.

redshift at which that patch was first reionized (since fossils from higher redshift have lower entropy, as in Fig 2).

The chief driver of high-redshift 21cm proposals has of course been to observe the IGM itself in 21cm emission (Madau, Meislin & Rees 1997; Tozzi et al 2000; Ciardi & Madau 2003). We note that if the filling factor of fossil HII regions is large, conditions are very favorable for such observations. Provided  $T_S \rightarrow T_K$  in the IGM, the only condition for the IGM to be seen in 21cm emission against the CMB is for  $T_K \gg T_{\text{CMB}}(z_{\text{obs}})$ . This is certainly satisfied in fossil HII regions. It was previously thought that recoil heating from Ly $\alpha$  photons could heat neutral regions (Madau, Meislin & Rees 1997), but a detailed calculation (Chen & Miralda-Escude 2003) shows the heating to be insufficient. In that case, a high-redshift X-ray background would be required to heat neutral regions. Such concerns are moot if a period of early reionization took place (as seems to be indicated by *WMAP* observations), followed by recombination: large tracts of warm, largely neutral gas would exist. Note, however, that brightness temperature fluctuations can only be detected if the contribution from unresolved radio point sources (Tozzi et al 2000; Oh & Mack 2003) can be successfully removed by using spectral structure in frequency space.

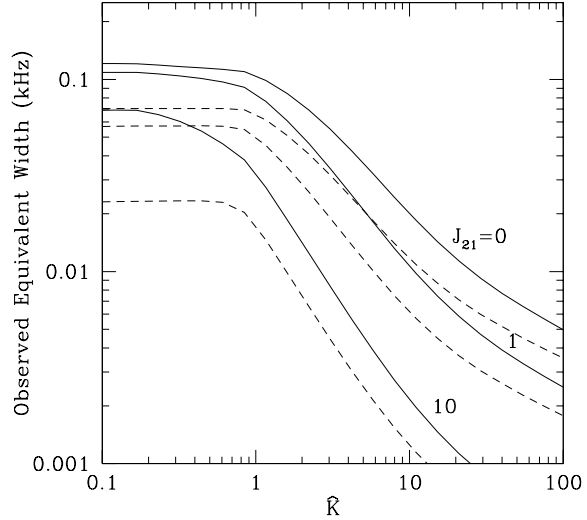


**Figure 14.** The observed 21cm absorption equivalent width of a  $2 \times 10^6 M_\odot h^{-1}$  halo at  $z = 10$ , for  $J_{21} = 0, 1, 10$ , as a function of  $\hat{K}$ . Solid lines are for an impact parameter of  $\alpha = 0.3r_{\text{vir}}$ , while dashed lines are for  $\alpha = 0.7r_{\text{vir}}$ . The equivalent width falls rapidly as the entropy floor rises; for the expected value of  $\hat{K} = 50$  at this redshift, equivalent widths are very small.

## 5 EFFECTS ON GLOBAL REIONIZATION SCENARIOS

### 5.1 General Considerations

We next address the effect of the suppression of mini-halo formation on the global reionization history. The importance of the effect depends on (1) the synchronization of the formation of mini-halos  $t_{\text{sync}}$  relative to the typical lifetime  $t_{\text{ion}}$  of the ionizing source, which determines the fraction of mini-halos subjected to feedback, as well as (2) on the recombination time  $t_{\text{rec}}$  relative to  $t_{\text{sync}}$ , which determines how long the ionized regions last and thus the fraction of active (as opposed to fossil) ionized regions at any given time.

In the limit of  $t_{\text{sync}} \ll t_{\text{ion}}$ , the fossil HII regions would appear only after all the mini-halos had already formed, and hence the feedback would have no effect on the total amount of reionization by mini-halos. In the absence of any other feedback effects, the IGM could then, in principle, be fully reionized by mini-halos, given a high enough ionizing photon production efficiency (although would subsequently recombine).

In the opposite limit,  $t_{\text{sync}} \gg t_{\text{ion}}$ , the contribution of mini-halos to reionization will be strongly suppressed. We can obtain a rough estimate for the maximum fraction of the IGM that can be ionized by the mini-halos. During the lifetime of its resident ionizing source, each mini-halo produces an ionized volume  $V_{\text{HII}}$ , which will correspond to the total number  $N_\gamma$  of ionizing photons injected into the IGM, i.e.  $\bar{n}V \approx N_\gamma$ , where  $\bar{n}$  is the mean hydrogen density. To a good approximation, recombinations can be ignored in this phase, since massive stars have lifetimes shorter than the

recombination time,  $t_{\text{rec}} \approx 3 \times 10^7 [C(1+z)/25]^{-3}$  years (see Fig. 15 below). On the other hand, the recombination time is shorter than the Hubble time,  $t_{\text{rec}}/t_{\text{hub}} \approx [C(1+z)/11]^{-1.5}$ , so in general, at high redshift  $z > 10$ , and for clumping factors  $C > 1$ , the ionized volume will recombine once its driving source turns off.

As argued above, for the purpose of the mini-halo suppression, we may nevertheless simply imagine that the HII region never recombines. Ignoring recombinations inside the ionized region, this is equivalent to setting the size of the fossil HII region to be the maximum (comoving) size of the active HII region, reached at the time when the ionizing source turns off.

The evolutions of the radii of the active and fossil HII regions are illustrated in Figure 15 for a single  $10^3 M_{\odot}$  metal-free star that turns on at  $z = 25$ . We follow the expansion of the ionization front  $R_S$  by solving the standard differential equation, taking into account ionizations, recombinations, and the Hubble expansion (e.g. Shapiro & Giroux 1987; Cen & Haiman 2000). We assume a constant clumping factor of  $C = 1$  (upper solid curve) or  $C = 10$  (lower solid curve). We assume further that the metal free star emits 40,000 ionizing photons per stellar proton at a constant rate for  $\sim 3 \times 10^6$  years (Tumlinson & Shull 2000; Bromm, Kudritzki & Loeb 2001; Schaerer 2002). Once the ionizing source turns off, the solid curves show the formal solution for the evolution of the ionization front.<sup>4</sup> The dashed curves show the size of the fossil HII region.

We can next consider the evolution of the volume filling factor of the fossil HII regions from the ensemble of mini-halos, and define the epoch  $z_f$  when the filling factor of these fossils reaches unity. As argued above, no new mini-halos can form at  $z < z_f$ . At this epoch, the global ionized fraction will be smaller than unity, because each fossil HII region has already partially recombined. Thus the global ionized fraction will be  $\sim \exp(-t_{\text{sync}}/\bar{t}_{\text{rec}})$ , assuming that the sources typically turned off a time  $t_{\text{sync}}$  ago, and  $\bar{t}_{\text{rec}}$  is the average recombination time over the interval  $t_{\text{sync}}$ . For example, assuming that the fossil HII regions overlap at  $z_f = 20$ , with the typical sources born at  $z = 25$ , and the recombination time evaluated at  $z = 22.5$  (with  $C = 1$ ), we find  $t_{\text{sync}} \approx \bar{t}_{\text{rec}} \approx 5 \times 10^7$  years, and a maximal ionized fraction of  $\sim 30\%$ .

## 5.2 Models for the Reionization History

To refine the above considerations, we next compute the evolution of the global ionized fraction using a semi-analytical model adopted from Haiman & Holder (2003, hereafter HH03). For technical details, the reader is referred to that paper. Here we only briefly summarize the main ingredients of the model, and describe the modifications we made to

<sup>4</sup> This formal solution predicts a shrinking of the ionization front. In reality, once the source turns off, recombinations throughout the ionized region will decrease the ionized fraction uniformly by the factor  $[R_S/R_{S,\text{max}}]^3$ , rather than reduce the size of a highly ionized volume. However, for our purposes of computing the global ionized fraction, the two interpretations are equivalent.

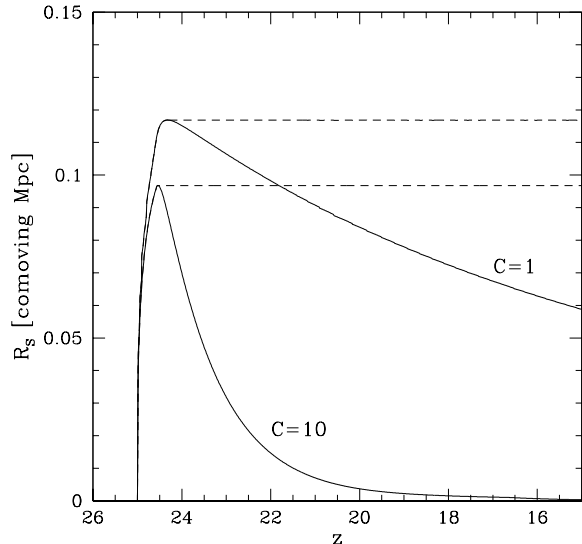


**Figure 15.** The evolution of comoving radius of the ionized region around a single  $10^3 M_{\odot}$  metal-free star that turns on at  $z = 25$ , and is assumed to emit 40,000 ionizing photons in  $\sim 3 \times 10^6$  years. The upper and lower solid curves show solutions that include recombinations with  $C = 1$  and  $C = 10$ . The ionized volume shrinks (or equivalently, the ionized fraction is decreased by the factor  $[R_S/R_{S,\text{max}}]^3$ ) after the source turns off at  $z \sim 24$ . The corresponding dashed curves show the radii of the fossil HII regions; these are assumed to stall at the maximum radius of the HII sphere and stay constant thereafter.

include the suppression of the formation of new mini-halos inside fossil HII regions.

In this model, we follow the volume filling fraction  $F_{\text{HII}}$  of ionized regions, assuming that discrete ionized Strömgren spheres are being driven into the IGM by ionizing sources located in dark matter halos. For simplicity, we ignore Helium in this work. The dark matter halo mass function is adopted from Jenkins et al. (2001). We consider two distinct types of ionizing sources, located in halos with virial temperatures of  $10^2 \text{ K} \lesssim T_{\text{vir}} \lesssim 10^4 \text{ K}$  (mini-halos) or  $T_{\text{vir}} \gtrsim 10^4 \text{ K}$  (large halos). We assume that in mini-halos, a fraction  $f_* = 0.005$  of the baryons turn into metal free stars (Abel, Bryan & Norman 2000, 2002; Bromm, Coppi & Larson 1999, 2002), which produce  $N_{\gamma} = 40,000$  ionizing photons per baryon, and  $f_{\text{esc}} = 100\%$  of these photons escape into the IGM. The product  $\epsilon \equiv f_* f_{\text{esc}} N_{\gamma} = 200$  determines the size of the ionized regions around mini-halos. For large halos, we adopt  $f_* = 0.1$ ,  $f_{\text{esc}} = 20\%$ , and  $N_{\gamma} = 4,000$ , for a total efficiency  $\epsilon = 80$ . In contrast with HH03, we here do not distinguish halos with  $10^4 \text{ K} < T_{\text{vir}} < 2 \times 10^5 \text{ K}$  from  $T_{\text{vir}} > 2 \times 10^5 \text{ K}$  (see Dijkstra et al. 2003 for the reason why this distinction is likely unimportant).

As in HH03, we then follow the evolution of the global ionized fraction  $F_{\text{HII}}(z)$  by summing the ionized volumes surrounding the individual dark matter halos. We exclude the formation of mini-halos in active ionized regions (but assume larger halos are impervious to photoionization feed-

back). The evolution of  $F_{\text{HII}}$  in this model is shown by the upper thin solid curve in Figure 16 (with  $C = 1$  in the upper panel, and  $C = 10$  in the lower panel). As the figure shows, in the absence of other feedback effects (see discussion in Haiman, Abel & Rees 2000 and Haiman 2003 for other feedback effects), the mini-halos could ionize the IGM in full by  $z \sim 14$  ( $C = 1$ ), or nearly fully by  $z \sim 10$  (if clumping is assumed to be more significant,  $C = 10$ ).

We next compute  $F_{\text{HII}}$  in the same model, except that we exclude the formation of new mini-halos in fossil HII regions. This is easily accomplished in practice: the suppression factor  $(1 - F_{\text{HII}})$  for the formation rate of mini-halos is replaced by a factor  $(1 - F'_{\text{HII}})$ . Here the fossil filling factor  $F'_{\text{HII}}$  is computed the same way as the ionized fraction  $F_{\text{HII}}$ , except that the individual ionized regions are assumed to follow the dashed curves from Figure 15 rather than the solid curves. In Figure 16, we show the evolution of the volume filling factor  $F'_{\text{HII}}$  of the fossil HII regions (dashed curves), as well as the reionization history  $F_{\text{HII}}(z)$  as the thick solid curves. Finally, for reference, we show  $F_{\text{HII}}(z)$  with mini-halos completely excluded ( $\epsilon = 0$ ) as the lower thin solid curves.

As apparent from Figure 15, the exclusion of new mini-halo formation from the fossil HII regions causes a significant suppression of the total ionized fraction that can be reached by mini-halos. Under the rather optimistic set of assumptions described by the thick solid curve in the upper panel, the maximum ionized fraction that can be reached is  $\sim 40\%$ . In reality, clumping is unlikely to be unity in the immediate vicinity ( $\lesssim 100$  kpc) of the ionizing sources (Haiman, Abel & Madau 2000).

The total electron scattering optical depth attributable to mini-halos (the appropriately weighted integral between the thick solid curve and the lower thin solid curve) is  $\tau = 0.07$  and  $\tau = 0.014$  in the  $C = 1$  and  $C = 10$  cases, respectively. This makes it unlikely that mini-halos can fully account for the large optical depth  $\tau = 0.17$  measured by *WMAP*. Note the thick curve in the upper panel of Figure 16 has a total  $\tau = 0.2$  ( $\tau = 0.07$  attributable to minihalos, and  $\tau = 0.13$  to larger halos), so that it is consistent with the *WMAP* measurement. Note that raising the efficiencies in mini-halos would not increase the optical depth attributed to minihalos, since feedback then would set in earlier (we have explicitly verified that  $\tau$  is approximately independent of efficiencies over a range of multiplicative factors 0.1 - 10 for  $\epsilon$ ). Finally, note that the suppression considered here and shown in Figure 16 provides a negative feedback *in addition* to the negative feedback expected from  $\text{H}_2$  photodissociation (Haiman, Rees & Loeb 1997; Haiman, Abel & Rees 2000). In fact, as discussed above, preheating *amplifies* the effect of the  $\text{H}_2$ -photodissociative negative feedback.

Because an entropy floor essentially eliminates gas clumping due to mini-halos (as shown in section 4.1), the reionization history is likely to more closely approximate the  $C=1$  case than the  $C=10$  case until low redshifts  $z < 10$  (when gas clumping due to larger structures predominates). An entropy floor therefore has two countervailing effects on reionization: by suppressing star formation in mini-halos, it reduces the comoving emissivity. However, by reducing gas

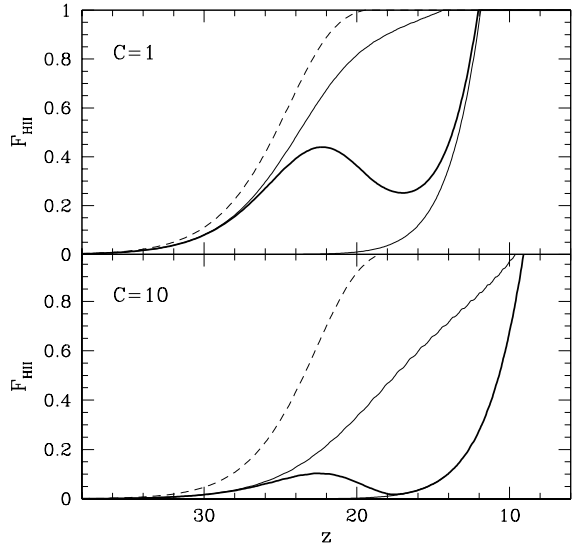


**Figure 16.** The evolution of the volume filling fraction  $F_{\text{HII}}$  of ionized hydrogen in reionization models with different assumptions about feedback on mini-halo formation. The upper and lower panels assume constant clumping factors of  $C = 1$  and  $C = 10$ , respectively. In both panels, the dashed curves show the volume filling fraction of the fossil HII regions. The thick solid curves show the evolution of  $F_{\text{HII}}$  assuming that mini-halos cannot form inside fossil HII regions. The upper solid curves assume that mini-halos are only excluded from forming inside active ionized regions. Finally, the lower solid curves ignore the contribution to  $F_{\text{HII}}$  from any mini-halos.

clumping, it also reduces the photon budget required for reionization. It is interesting to note that the evolution of the filling factor is non-monotonic for the  $C=1$  case: feedback due to early reionization naturally produces a bump in the comoving emissivity, and a pause ensues before larger halos (which can resist feedback) collapse. This is similar to the reionization histories derived by (Cen 2003; Wyithe & Loeb 2003), but is regulated by feedback from the entropy floor rather than a Pop III to Pop II transition due to a universal metallicity increase.

## 6 CONCLUSIONS

In this paper, motivated by the *WMAP* results, we have considered the feedback effect of early reionization/preheating on structure formation. This feedback effect is *inevitable* in any reionization scenario in which star formation throughout the universe is not completely synchronized. Our principal conclusions are as follows:

1. Fossil HII regions have a residual entropy floor after recombination and Compton cooling which is *higher* than the shock entropy for mini-halos ( $T_{\text{vir}} < 10^4 \text{K}$ ); thus, such halos accrete gas isentropically. The IGM entropy depends primarily on the redshift and only weakly on the overdensity  $\delta$ ; it is thus largely independent of the details of structure formation. For this reason, and also because it is con-



served during adiabatic accretion or Hubble expansion, the gas entropy is a more fundamental variable to track than the temperature. We provide a simple analytic formula for the temperature (and hence entropy  $K = T/n^{2/3}$ ), in equations 33 and 35. An early X-ray background would also heat the entire IGM to similarly high adiabats. The entropy floor due to the latter would be much more spatially uniform.

2. We apply the entropy formalism used to calculate the effect of preheating on low-redshift galaxy clusters to the high-redshift minihalos. We obtain detailed gas density and pressure profiles, which we use to calculate the impact of preheating on the central density, accreted gas fraction, gas clumping factor, and mini-halo baryonic mass function.

3. These quantities can then be used to calculate global effects of preheating. The collapsed gas fraction in minihalos falls by  $\sim 2$  orders of magnitude, while the gas clumping factor falls to  $C \rightarrow 1$ , as for a uniform IGM. An entropy floor reduces the photon budget required for full reionization by about an order of magnitude, by reducing gas clumping and eliminating the need for mini-halos to be photo-evaporated before reionization can be completed.

4. However, an entropy floor does not necessarily promote early reionization: it also sharply reduces the comoving emissivity. By reducing the central gas densities in minihalos, preheating impedes  $H_2$  formation and cooling, and reduces the critical UV background required for  $H_2$  suppression by 2-4 orders of magnitude. *Thus, once a comoving patch of the IGM is reionized, no subsequent star formation in mini-halos can take place in that volume.* The patch can only be reionized by more massive halos  $T > 10^4 K$ , which can undergo atomic cooling. By furnishing an entropy floor, X-rays also suppress  $H_2$  formation. Thus, contrary to conventional wisdom, X-rays provide negative rather than positive feedback for early star formation.

5. Mini-halos will not be observable in 21cm emission/absorption in fossil HII regions. Thus, 21cm observations provide an unusual probe of the topology of reionization: mini-halos trace out regions of the IGM which have *never* been ionized. If mini-halos are seen in large numbers, this places an upper limit on the filling factor of fossil HII regions and the X-ray background at that redshift.

6. We have computed the reionization histories as in HH03, but taking the feedback effect of an entropy floor (and reduction of gas clumping) into account. The strong feedback in fossil HII regions imply that HII fronts at high redshift never overlap, and global reionization at high redshift does not occur. This limits the contribution of mini-halos to the reionization optical depth  $\tau < 0.07$ , almost independent of star formation efficiency in mini-halos (if star formation is more efficient, feedback sets in earlier). Thus, the bulk of the optical depth observed by WMAP must come from more massive objects.

7. Strikingly, we obtain a double-peaked reionization history: an early peak in which the universe is filled with fossil HII regions, followed by a pause before more massive halos collapse which finally fully reionize the universe. This is similar to 'double reionization' scenarios computed by other authors (e.g. Cen (2003); Wyithe & Loeb (2003)), but one in which the the comoving emissivity is regulated by gas en-

tropy, rather than a Pop III to Pop II transition due to a universal metallicity increase. This last point deserves additional comment. A metallicity-regulated evolution of the emissivity requires that metal pollution is fairly spatially uniform. However, different parts of the IGM likely undergo the Pop III to Pop II transition at different epochs. Furthermore, an increase in metallicity does not necessarily result in a drop in the overall emissivity: metal line cooling likely results in a larger star formation efficiency in halos, since metals are not subject to internal UV photo-dissociation, unlike  $H_2$ . The factor of  $\sim 10$  drop in the HI ionizing emissivity per stellar baryon could be outweighed by the increase in the total mass of stars formed. In comparison, we argue that an entropy-regulated transition is inevitable, and therefore more robust. This is an important conclusion, given the possibility that future CMB polarization studies will be able to distinguish among different reionization histories (HH03; Holder et al 2003).

In this semi-analytic study, we essentially assumed a single value of the entropy floor at each redshift, for all halos. In reality, as we discussed above, there should be large fluctuations in entropy, depending on the topology/history of reionization and the accretion/merger history of halos. It would be interesting to study these effects in detail in three dimensional numerical simulations. To begin with, it would be interesting to re-run existing simulations of the collapse of gas in mini-halos, but adding an entropy floor in the initial conditions. Such studies could quantify more precisely the effects of an entropy floor in suppressing  $H_2$  formation and cooling in mini-halos. In fact, since densities are lower and gas cooling is reduced, it should be a computationally more tractable problem. With the aid of larger volumes, several global issues mentioned above could be addressed: for instance, a global, self-consistent study of feedback as in Machacek, Bryan & Abel (2001), but including the effects of both the entropy floor *and* UV feedback. Because of its strong effect on the evolution of the comoving emissivity, gas entropy acts as a self-regulating mechanism which likely has a strong influence in controlling the progress of reionization.

## REFERENCES

- Abel T., Bryan G.L., Norman M.L., 2000, ApJ, 540, 39  
 Abel, T., Bryan, G. L., & Norman, M. L. 2002, Science, 295, 93  
 Allison, A.C., & Dalgarno, A., 1969, ApJ, 158, 423  
 Babul, A., Balogh, M.L., Lewis, G.F., Poole, G.B., 2002, MNRAS, 330, 329  
 Barkana, R., & Loeb, A., 1999, ApJ, 523, 54  
 Barkana, R., & Loeb, A., 2002, ApJ, 578, 1  
 Barkana, R., & Loeb, A., 2002, ApJ, 578, 1  
 Balogh, M.L., Babul, A., & Patton, D.R., 1999, MNRAS, 307, 463  
 Benson, A.J., Lacey, C.G., Baugh, C.M., Cole, S., Frenk, C.S., 2002, MNRAS, 333, 156  
 Bromm, V., Coppi, P. S., & Larson, R. B. 1999, ApJ, 527, 5  
 Bromm, V., Ferrara, A., Coppi, P.S., & Larson, R.B. 2001, MNRAS, 328, 969  
 Bromm V., Coppi P.S., Larson R.B., 2002, ApJ, 564, 23  
 Bromm, V., Kudritzki, R. P., & Loeb, A. 2001, ApJ, 552, 464

- Bullock, J.S., Kravtsov, A.V., & Weinberg, D.H., 2000, ApJ, 539, 517
- Cen, R. 2003, ApJ, submitted, astro-ph/0210473
- Cen, R., & Haiman, Z. 2000, ApJ, 542, L75
- Chen, X., & Miralda-Escude, J., 2003, ApJ, submitted, astro-ph/0303395
- Ciardi, B., Ferrara, A., & Abel, T. 2000, ApJ, 533, 594
- Ciardi, B., & Madau, P., 2003, ApJ, submitted, astro-ph/0303249
- Dijkstra, M., et al. 2003, in preparation
- Elvis, M., et al, 1994, ApJS, 95, 1
- Gnedin, N.Y., 2000, ApJ, 542, 535
- Fixsen, D. J., & Mather, J. C. 2002, ApJ, 581, 817
- Frenk, C., et al, 1999, ApJ, 525, 554
- Furlanetto, S.R., & Loeb, A., 2002, ApJ, 571, 1
- Haiman, Z. 2003, in Carnegie Symposium Review Series I, ed. L. Ho.
- Haiman, Z., Abel, T., & Rees, M. J. 2000, ApJ, 534, 11
- Haiman, Z., Abel, T., & Madau, P. 2001, ApJ, 551, 559
- Haiman, Z., & Holder, G. 2003, ApJ, in press, astro-ph/0302403 (HH03)
- Haiman, Z., Rees, M. J., & Loeb, A. 1996, ApJ, 467, 522
- Haiman, Z., Rees, M. J., & Loeb, A. 1997, ApJ, 476, 458 [erratum: 1997, ApJ, 484, 985]
- Haiman, Z., Spergel, D.N., & Turner, E.L., 2003, ApJ, 585, 630
- Hansen, S., & Haiman, Z. 2003, ApJL, submitted, astro-ph/0305126
- Hellsten, U., & Lin, D.N.C., 1997, astro-ph/9708086
- Holder, G., Haiman, Z., Kaplinghat, M., & Knox, L. 2003, ApJ, in press, astro-ph/0302403
- Iliev, I.T., Shapiro, P.R., Ferrara, A., & Martel, H., 2002a, ApJ, 572, L123
- Iliev, I.T., Scannapieco, E., Martel, H., & Shapiro, P.R., 2002b, MNRAS, submitted, astro-ph/0209216
- Kogut A. et al, 2003, ApJ, submitted; astro-ph/0302213
- Knox, L., Scoccimarro, R., & Dodelson, S., 1998, PhRvL, 81, 2004
- Machacek, M. E., Bryan, G. L., Abel, T. 2001, ApJ, 548, 509
- Madau, P., Meisner, A., & Rees, M.J., 1997, ApJ, 475, 429
- Madau, P., Ferrara, A., & Rees, M.J. 2001, ApJ, 554, 92
- Magliocchetti, M., Salvaterra, R., & Ferrara, A., 2003, MNRAS, 342, L25
- Navarro, J.F., Frenk, C.S., & White, S.D.M., 1997, ApJ, 490, 493
- Oh, S.P., 1999, ApJ, 527, 16
- Oh, S.P., 2000, PhD thesis, Princeton University, Chapter 4.
- Oh, S.P., 2001, ApJ, 553, 25
- Oh, S.P., & Benson, A., 2003, MNRAS, 342, 664
- Oh, S.P., & Haiman, Z., 2002, ApJ, 569, 558 (OH02)
- Oh, S.P., & Mack, K., 2003, MNRAS, submitted, astro-ph/0302099
- Oh, S.P., Cooray, A., & Kamionkowski, M., 2003, MNRAS, 342, L20
- Ricotti, M., Gnedin, N.Y., & Shull, J.M., 2002, 575, 49
- Rosati, P., Borgani, S., & Norman, C., 2002, ARAA
- Santos, M.R., Bromm, V., Kamionkowski, M., 2002, MNRAS, 336, 1082
- Santos, M. G., Cooray, A., Haiman, Z., Knox, L., & Ma, C.-P. 2003, ApJ, submitted, astro-ph/0305471
- Schaerer, D. 2002, A&A, 382, 28
- Shapiro, P., & Giroux, M. L. 1987, ApJ, 321, L107
- Shapiro, P.R., Iliev, I.T., Raga, A.C., 1999, MNRAS, 307, 203
- Shapiro, P. R., Raga, A. C., & Mellema, G. 1998, in Molecular Hydrogen in the Early Universe, Memorie Della Societa Astronomica Italiana, Vol. 69, ed. E. Corbelli, D. Galli, and F. Palla (Florence: Soc. Ast. Italiana), p. 463
- Shapiro, P.R., Iliev, I.T., Raga, A.C., Martel, H., 2003, in The Emergence of Cosmic Structure, 13th Annual October Astro-physics Conference in Maryland, S. Holt & C. Reynolds, eds (AIP), in press, astro-ph/0302339
- Shull, J.M., & van Steenberg, M.E., 1985, ApJ, 298, 268
- Somerville, R.S., 2002, ApJ, 572, L23
- Spergel D.N. et al, 2003, ApJ, submitted, astro-ph/0302209
- Tegmark, M., Silk, J., Rees, M.J., Blanchard, A., Abel, T., Palla, F., 1997, ApJ, 474, 1
- Tozzi, P., & Norman, C., 2001, ApJ, 546, 63
- Tozzi, P., Madau, P., Meisner, A., & Rees, M.J., 2000, ApJ, 528, 597
- Tumlinson, J., & Shull, M. J. 2000, ApJ, 528, L65
- Venkatesan, A., Giroux, M.L., Shull, J.M., 2001, ApJ, 563, 1
- Voit, G.M., Bryan, G.L., Balogh, M.L., Bower, R.G., 2002, ApJ, in press, astro-ph/0205240
- Wyithe, S., & Loeb, A. 2003, ApJ, 586, 693

## APPENDIX I: ANALYTIC EXPRESSION FOR THE FINAL TEMPERATURE

It is useful to have an approximate analytic expression for the final temperature of a parcel of gas cools down to, given the initial temperature  $T_i$ , redshift  $z$ , overdensity  $\delta$  and length of time spent cooling  $t$ . This allows one to quickly estimate the effect of early reionization in different situations without evolving the full chemistry code. We develop such an expression in this Appendix.

At the redshifts and overdensities of interest, Compton cooling dominates by far. The most relevant physics is Compton cooling and hydrogen recombination:

$$\dot{T} = -\frac{8}{3} \frac{aT_\gamma^4 \sigma_T}{m_e c} \frac{x_e}{1+x_e} (T - T_\gamma) \quad (32)$$

$$\dot{x}_e = -x_e^2 n \alpha$$

Note that  $(T - T_\gamma) \approx T$  since  $T \gg T_\gamma$ , and  $\alpha \propto T^{-0.7}$  in the temperature range of interest. Assuming the gas is fully ionized  $x_e = 1$  at some initial temperature  $T_i$ , we obtain the analytic solution:

$$T(x_e) = T_i \left[ 1 + 1.4A \left( \ln \left( \frac{1+x_e}{x_e} \right) - \ln(2) \right) \right]^{-1/0.7} \quad (33)$$

where

$$A \equiv \frac{4}{3} \frac{aT_\gamma^4 \sigma_T}{n \alpha(T_i) m_e c} = \frac{t_{rec}(T_i)}{t_C} \propto \frac{(1+z)}{\delta} T_i^{0.7} \quad (34)$$

This gives temperature as a function of ionization fraction  $x_e$ . We therefore need to know the final ionization fraction. How can we estimate it? If the gas recombines isothermally at temperature  $T'$ , the ionization fraction is given by:

$$x_e(t) = \frac{x_o}{1 + (t/t_{rec}(T'))} \quad (35)$$

where  $x_o = 1$  is the initial ionization fraction. If the gas cools as it recombines, substituting the instantaneous temperature  $T'$  into the expression, would overestimate the speed of recombination and underestimate  $x_e$ . We find that if we substitute  $T' = 2T$  and substitute this into equation 33, the solution of this non-linear equation for  $T_f$  is remarkably close to the full non-equilibrium solution (see points in Figure 1). We have also verified that we obtain fairly accurate results for  $x_e(t)$ . Equations 33 and 35 thus give  $T_f(z, \delta, T_i, t)$ .

Our neglect of recombination line cooling fails in high density regions. This leads to at most a factor  $\sim 2$  error in the final temperature, since recombination line cooling can cool gas down to at most  $\sim 5000\text{K}$ . The entire discussion assumes that  $\text{H}_2$  formation and cooling is not competitive with Compton cooling, which is generally true in low density regions.